Coupling between CO_2, water vapor, temperature, and radon and their fluxes in an idealized equilibrium boundary layer over land

Alan K. Betts
Atmospheric Research, Pittsford, Vermont, USA

Brent Helliker and Joe Berry
Department of Global Ecology, Carnegie Institution of Washington, Stanford, California, USA

Received 5 December 2003; revised 8 April 2004; accepted 22 June 2004; published 17 September 2004.

[1] We propose a new approach for relating concentration measurements in the atmospheric boundary layer to surface fluxes based on a simple equilibrium boundary layer model (an extension of *Betts* [2000]). This is a major shift from the traditional focus on the growth of the daytime dry boundary layer. We show equilibrium solutions for the diurnally averaged properties of the boundary layer that link the mixed layer equilibrium (on timescales longer than a day) of potential temperature, water vapor, CO_2 (and other trace gases such as radon) with an interactive cloud layer and with the surface energy, water, and carbon balance. We examine these processes as a function of a set of external parameters: soil water content, which directly impacts respiration and photosynthesis, and hence transpiration; the surface net shortwave, directly linked to net radiation, which is also coupled to photosynthesis and transpiration; and the radiative cooling of the mixed layer (ML), which in the equilibrium model directly affects the surface sensible heat. We also show solutions where the net shortwave and radiative cooling are coupled to the cloud field. Our other variable model parameters are the properties of air entrained into the CBL, the midtropospheric values of vapor mixing ratio, CO_2 and radon, and the lapse rate above cloud base. We considered two idealized ecosystems: forest (based on observations in Wisconsin) and grassland (using parameter estimates from the literature) to show how the vegetation model affects the ML equilibrium. We show how the mass transport out of the subcloud layer and the mass exchange with the free troposphere couples the mixed layer equilibrium of water vapor, CO_2, and radon with the corresponding surface fluxes. We suggest that regional ML budgets may give useful constraints on regional carbon budgets, and that the coupling with the cloud field is a fundamental part of the ML equilibrium. *INDEX TERMS:* 1818 Hydrology: Evapotranspiration; 1615 Global Change: Biogeochemical processes (4805); 3307 Meteorology and Atmospheric Dynamics: Boundary layer processes; 3322 Meteorology and Atmospheric Dynamics: Land/atmosphere interactions; *KEYWORDS:* boundary layer, CO_2 fluxes, energy and water fluxes

Citation: Betts, A. K., B. Helliker, and J. Berry (2004), Coupling between CO_2, water vapor, temperature, and radon and their fluxes in an idealized equilibrium boundary layer over land, *J. Geophys. Res.*, *109*, D18103, doi:10.1029/2003JD004420.

1. Introduction

[2] There is a current initiative in the carbon cycle community to develop methods to resolve regional to continental scale net CO_2 fluxes, largely in an effort to constrain larger scale estimates of the global carbon budget. Past efforts to obtain regional scale estimates of CO_2 flux have concentrated on the atmospheric boundary layer (ABL) as the regional flux integrator [*Raupach et al.*, 1992; *Denmead et al.*, 1996; *Levy et al.*, 1999; *Kuck et al.*, 2000; *Lloyd et al.*, 2001]. The links between surface transpiration, ML depth and climate over the seasonal cycle are well established [*Fitzjarrald et al.*, 2001]. Accurate ABL budgets are often constrained experimentally by accounting for flux divergence in the horizontal and through-cloud flux in the vertical [*Fitzjarrald*, 2002]. However, boundary layer budgets are difficult to close over the diurnal time scale, and a current focus is on coupling measurements with models that properly simulate the complex dynamics of the lower atmosphere over the diurnal cycle. On the other hand, the short-term dynamics of the ABL, when viewed over longer time scales, are captive to larger-scale processes that link the ascending and descending branches of the atmospheric general circulation. For example, it has been estimated that this flow of air from the ABL to the upper troposphere taken globally is sufficient to vent the total volume of the ABL in approximately 4 days [*Cotton et al.*, 1995]. This upward circulation is closed by subsi-

0148-0227/04/2003JD004420$09.00

dence, in which tropospheric air sinks as it cools radiatively and is entrained back into the ABL. Viewed in this context, the properties of the ABL averaged over several days should be near a steady state in which there is a rough balance in energy terms between surface evaporation and other energy fluxes and the large scale subsidence of warm dry air into the ABL. In this paper we explore the implications of these thermodynamic constraints on the boundary layer for interpreting the concentration of carbon cycle and other gases in the boundary layer. In our opinion, this argument is important because it provides a rationale for making flux measurements based on long-term averages of ABL properties. Two recent studies [*Bakwin et al.*, 2004; *Helliker et al.*, 2004] have demonstrated that the monthly average gradient in CO_2 concentration between the ABL and the adjacent free troposphere and a corresponding estimate of vertical velocity at the top of the ABL yield reasonable estimates of net CO_2 flux integrated over monthly intervals. Furthermore, if this argument is correct then it follows that models which correctly simulate the short-term dynamics of the lower atmosphere may not be sufficient to understand the CO_2 balance of the ABL over intervals longer than a few days, unless they represent the circulations on these longer timescales correctly.

[3] Over the oceans the diurnal cycle is small, and *Betts and Ridgway* [1989] proposed an equilibrium approach to the ABL budgets of water and energy, in which the radiatively driven subsidence, radiative cooling and the surface fluxes are in balance. The tropical circulation has broad regions where large-scale subsidence caps a remarkably uniform convective boundary layer (CBL) of shallow nonprecipitating cumulus clouds (the "trade winds"). Here the subsidence of dry air balances the large surface evaporation, while the radiative cooling of the moist CBL is balanced the subsidence of warm air though the inversion and a small surface sensible heat flux. This moist equilibrium CBL in turn feeds moisture to the precipitating convection in the ascending branches of the Hadley and Walker circulations, where the condensation heating lifts air in deep convective clouds to the upper troposphere. The circulation is closed in the subsiding trade wind branch, where air sinks at about 40 hPa day^{-1}, as it cools radiatively. So for the tropics as a whole, there is a rough balance in energy terms between surface evaporation, condensation heating, and net radiative cooling on timescales of a week or so [*Betts and Ridgway*, 1989]. Over the summer continents, away from the major monsoon circulations, there is also a rough balance between precipitation and evaporation. Consequently, *Betts* [2000] suggested a similar approach to the surface-ABL climate equilibrium over land by averaging over the diurnal cycle. He proposed an equilibrium model for the mixed subcloud layer (ML) over land, in which the diurnally averaged surface fluxes balance the fluxes through cloud base, and the other diabatic terms in the ML, such as radiative cooling and the evaporation of falling precipitation. This is the assumption that, as over the ocean, the ABL approaches a steady state or equilibrium between the surface and the overlying free troposphere, on timescales longer than a day. He showed the strong dependence of mean ML depth on vegetative resistance to evaporation, as well as the dependence on surface net radiative forcing. This idealized equilibrium boundary layer model [*Betts*, 2000] gave a reasonable representation of the observed trends with soil moisture of composite data from the First International Satellite Land Surface Climatology Project (ISLSCP) Field Experiment (FIFE), and the trends with soil moisture of daily mean surface data from the European Centre for Medium-Range Forecasts (ECMWF) reanalysis. *Betts* [2000] simply specified vegetative resistance as a parameter.

[4] In this paper we extend this equilibrium model by adding a model for photosynthesis and respiration, largely as a function of soil moisture and incident radiation, and with an observational basis. This couples the CO_2 and water vapor fluxes at the surface (through vegetative resistance), and enables us to discuss the coupling of CO_2 and mixing ratio, q, in the ML. In addition, we add a radon model with constant surface emission rate to show how this scalar is coupled to ML structure and fluxes of water and CO_2 on timescales longer than a day. Radon is a naturally produced radioactive gas emitted by soils, but not water bodies, and it has a short (3.8 day) half-life in the atmosphere. This means there is a strong gradient of radon between the surface and free troposphere, which depends on the ML depth and the coupling of the ML to the layer above. The transports of radon, water vapor and CO_2 out of the ML are coupled, but the surface fluxes are different, so we shall show that their different equilibria provide different insights into the ML budget. *Betts* [2000] closed the ML solutions by specifying lapse rate and relative humidity just above the ML, and by requiring ML top to coincide with cloud base. The model showed that in general the ML balance required a moisture flux into clouds, unless there was strong subsidence of rather dry air above the ML. Here we make two further extensions. We will define an equilibrium shallow cloud layer, so that we can couple the entire convective boundary layer (CBL) to the entrainment or mass exchange at the CBL top, where we specify "free tropospheric" values of mixing ratio, CO_2 and radon. We can then determine the entrainment rate that will satisfy equilibrium of both the subcloud ML and the CBL as a whole. This corresponds quite closely to the radiative equilibrium subsidence rate, so the model is conceptually workable. The second extension will be to couple the surface net shortwave and the ML radiative cooling to the net cloud mass flux.

[5] The inspiration for the first extension to couple to the free troposphere came from observations. In a companion paper, *Helliker et al.* [2004] show that the monthly average vertical gradients of CO_2 and mixing ratio between the ML and the free troposphere, coupled with a single vertical exchange velocity, were qualitatively representative of the corresponding surface fluxes: net ecosystem exchange (NEE) and evaporation, as measured by eddy covariance. In our equilibrium model, the CO_2 and water vapor fluxes are coupled exactly, and the entrainment rate that we derive has just the magnitude of the equivalent vertical exchange velocity of *Helliker et al.* [2004]. The coupling of the CO_2 and water vapor structure is very tight in the ML [e.g., *Betts*, 2003], and if this coupling can be extended to the entire CBL, then the

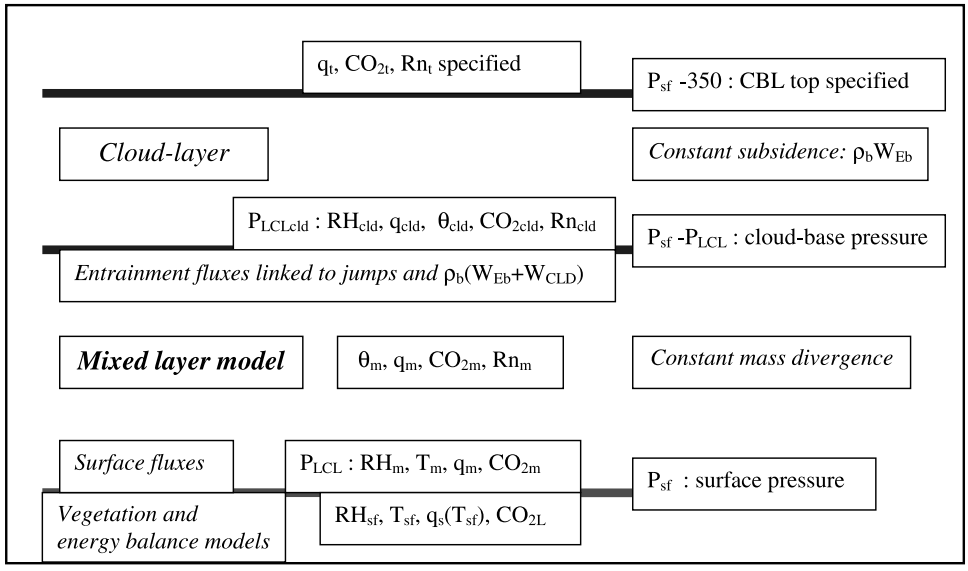

Figure 1. Conceptual structure of the equilibrium model. See color version of this figure in the HTML.

vertical gradients can be used to estimate the NEE from the surface evaporation. Precipitation of water from clouds complicates the use of the water budget, so we explore the information in the ML radon budget. The decay of radon in the ML and cloud layers introduces additional terms, but they can be estimated with some precision, so the radon budget may provide an additional independent estimate of the vertical mass exchange. Our equilibrium model provides a framework for interpreting data, and moves us closer to the goal of using the integrating effect of the CBL to improve regional-scale estimates net surface CO_2 flux, and surface evaporation.

[6] This equilibrium modeling approach represents a major conceptual shift from most of the research of the last two decades which has focused on the growth of the daytime dry BL and its mixing with the overlying atmosphere [*De Bruin*, 1983; *McNaughton and Spriggs*, 1986; *Raupach*, 1995, 2000, 2001]. *Raupach* [2000] shows that as the BL gets deeper, "equilibrium" is not reached within a semidiurnal timescale. Our 24-hour averaged model takes the perspective that the climate problem over land is fundamentally the description of the mean state (with a superimposed diurnal cycle) and the transition between these mean states, rather than the description of the daytime growing BL. In this paper, we present sensitivity studies of an idealized model without any observational validation or time-dependent modeling for comparison. However, *Betts* [2004] shows that the BL climate states over land and the coupling of processes at the surface in a fully time dependent model (the European Centre reanalysis) can be mapped with remarkable precision by the daily mean state and daily flux averages. Indeed although there is not strict equilibrium of the CBL on the 24-hour timescale, the nonstationarity can itself be seen in the fully time dependent system (as the CBL warms up on consecutive days, for example), and it is small.

[7] There is a second profound conceptual shift in this paper: that the climate equilibrium over land is tightly coupled to the cloud field. In contrast, the references cited above focused on the growing dry convective BL. In our simple model, we couple the ML to cloud base and the radiation field to the CBL clouds. Once again, the global modeling analysis [*Betts*, 2004] with fully interactive prognostic clouds supports this analysis, and indeed shows that the coupling from a climate perspective is with the entire cloud field. Essentially, the source of all clouds is evaporation at the surface, coupled though the BL to both shallow and deep convection; and midlevel clouds are often the decay products of earlier convective systems. Although the cloud coupling we present here is primitive, we hope to develop this further in future work. Since the sources and sinks for CO_2 are also at the surface, its fate is coupled to the cloud field in a similar way. The sensitivity studies presented here use illustrative vegetation model parameters, taken in part from Wisconsin forest data and for grassland from the literature, and they will not be representative of all ecosystems.

2. Idealized Equilibrium Model

[8] The conceptual framework of the model is summarized in Figure 1. It centers on a ML model for the subcloud layer, for which we shall determine the four variables: potential temperature, θ_m, mixing ratio, q_m, CO_{2m}, and radon mixing ratio, Rn_m. There is a vegetation and energy balance model at the surface. Some of the surface variables, relative humidity, RH_{sf}, temperature, T_{sf}, and saturation mixing ratio, $q_s(T_{sf})$ and CO_{2L} outside the leaf are shown, while others will be discussed later. Aerodynamic equations determine the surface fluxes from the gradients across the atmospheric surface layer, except for the radon flux that is specified. The thermodynamic variables at the base of the ML determine the lifting condensation level (LCL), which is taken as both cloud base and the top of the ML. Cloud base pressure is found as the difference of the surface pressure P_{sf} and the pressure thickness P_{LCL} to the LCL. At the top of the ML, the entrainment fluxes (which balance the surface fluxes for q and CO_2) are determined by the jumps in θ, q, CO_2 and radon; and a mass flux, which is

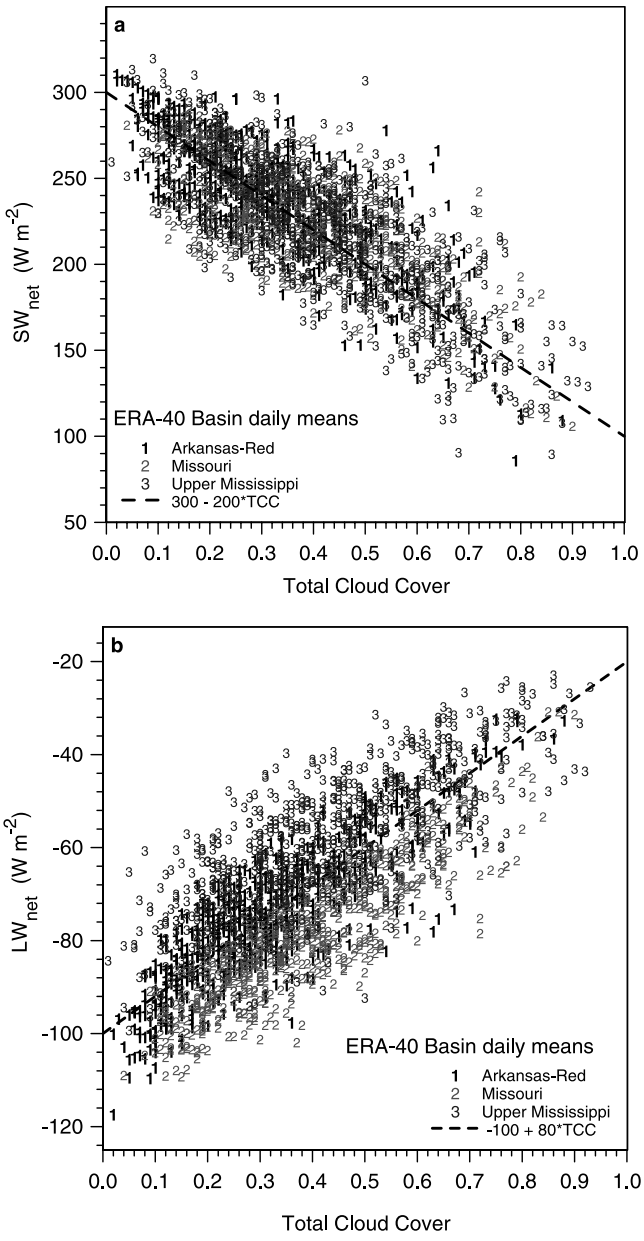

Figure 2. (a) Coupling between total cloud cover and daily mean surface net shortwave in basin averages of ERA-40. (b) As in Figure 2a for net longwave radiation. See color version of this figure in the HTML.

found from the equilibrium solution. We need values just above cloud base, suffix cld, which will be discussed later. We do not solve for the full structure of the cloud layer (which is assumed to be a nonprecipitating cumulus layer), so we specify a CBL top at a pressure 350 hPa below the surface pressure, where "midtropospheric" values of q, CO_2, and radon are specified as upper boundary conditions, suffix t. We are able to satisfy simple budget equations for q, CO_2, and radon for the whole CBL, by specifying a constant subsidence in the cloud layer (a value also determined from the equilibrium) with constant divergence in the mixed subcloud layer. The actual pressure thickness of the cloud layer only plays a role in the radon decay equation (see later). We shall now discuss each of the components of the model in turn.

2.1. Surface Energy Balance

[9] The surface fluxes satisfy an energy budget. The daytime balance, suffix D, for time period t_D, is

$$t_D * [SW_{netD} + LW_{netD} = R_{netD} = H_D + \lambda E_D + G_D], \quad (1)$$

where SW_{net}, LW_{net}, R_{net} are the net short-wave, long-wave and net surface radiative fluxes, H is the sensible heat flux, E the evaporation (which we shall later assume is stomatally controlled, so that our solutions do not represent disturbed conditions with evaporation off a wet canopy), λ is the latent heat of vaporization, and G is the ground heat flux and heat storage in the canopy. We neglect the energy needed for photosynthesis.

[10] The nighttime balance, suffix N, for time period t_N, is

$$t_N * [LW_{netN} = R_{netN} = H_N + \lambda E_N + G_N]. \quad (2)$$

Add (1) and (2) to get 24-hour total, and neglect net storage and night evaporation by setting

$$G_D * t_D + G_N * t_N + \lambda E_N * t_N = 0 \quad (3)$$

to give

$$R_{net24} * t_{24} = H_{24} * t_{24} + \lambda E_{24} * t_{24}. \quad (4)$$

We have defined 24-hour mean fluxes as follows:

$$R_{net24} * t_{24} = R_{netD} * t_D + R_{netN} * t_N = SW_{netD} * t_D + LW_{netD} * t_D + LW_{netN} * t_N \quad (5a)$$

$$H_{24} * t_{24} = H_D * t_D + H_N * t_N \quad (5b)$$

$$\lambda E_{24} * t_{24} = \lambda E_D * t_D. \quad (5c)$$

We express everything in terms of 24-hour fluxes, although we shall neglect evaporation at night by assuming E is photosynthetically controlled (see section 2.3). We absorb the typically downward nighttime sensible flux, which contributes to the stable BL at sunrise, into the 24-hour mean. This introduces a small hidden approximation, since the model of *Betts* [2000] couples H_{24} with an aerodynamic resistance to a skin-air temperature difference, so we are assuming a daytime, unstable transfer model for heat. One obvious extension would be to average over day and night separately. We have done this, but the solutions are not qualitatively different, so we do not present these solutions.

2.2. Radiative Fluxes

[11] We shall use only a simplified representation of the 24-hour short-wave and long-wave fluxes, which are needed to drive the energy balance (and in the next section, we couple photosynthesis to the shortwave flux). Figure 2 shows the coupling in model data between total cloud cover (TCC) and SW_{net24} (upper panel) and LW_{net24} (lower panel) from the ECMWF 40-year reanalysis (ERA-40) averaged over three Mississippi subbasins [see *Betts et al.*, 2003] for the months June, July, and August, 1993–1999. The SW relationship is independent of basin, and reasonably represented by the dashed line shown

$$SW_{net24} = 300 - 200 * TCC. \quad (6a)$$

Table 1. Vegetation Parameters

Vegetation	Forest	Grassland
LAI in (8)	5	3
E_{veg} in (10)	6	10
Q_{10} in (13)	1.9	2.2

For the long-wave flux there is some variation between the basins, related to temperature (the Mississippi is the coolest basin) and humidity (the Missouri is the driest basin), which we shall ignore, since we will not have a full model for the structure of the convective boundary layer (CBL). The dashed line fit shown is

$$LW_{net24} = -100 + 80 * TCC. \quad (6b)$$

Combining (6a) and (6b) couples the LW to the SW flux with the simple relation

$$LW_{net24} = 0.4 * (SW_{net24} - 50). \quad (6c)$$

We shall show solutions in which we specify SW_{net24} as an external parameter. Our BL model does not give solutions for cloud cover, but it will give a net cloud mass flux, and this will be used to give solutions in which SW_{net24} is coupled to the cloud field (see section 2.14). *Betts* [2004] gives a more extensive analysis of coupling of the cloud and BL structure in the ERA-40 data.

2.3. Photosynthetic Uptake Model

[12] We use a simplified canopy photosynthesis model, based initially on the work of *Monteith* [1977] and *Collatz et al.* [1991], and then fitted to observed eddy-covariance data from temperate mixed forest in northern Wisconsin [*Davis et al.*, 2003], in which photosynthesis is a function of incoming absorbed photosynthetic photon flux density (PPFD), leaf area index (LAI), with stress factors for temperature and relative humidity at the leaf, and soil moisture. We use different light use efficiency parameters representing forests and grasslands to obtain the full range of vegetative resistance seen in grassland and forest systems [*Kim and Verma*, 1990; *Betts et al.*, 1999]. The stomatal resistance to the evaporation of water is then computed from the photosynthetic flux and CO_2 gradient across the leaf.

[13] The equation set, which follows, were derived by fitting mean-daily average data from a forest site in Wisconsin [*Davis et al.*, 2003], so as to be consistent with the daily average equilibrium model. It is not our intent to provide a careful analysis of this data set, and we do not claim it will be represent other ecosystems. The idealized equilibrium model involves many simplifications, so our fits to the Wisconsin data are also simple. We obtain photosynthetic flux density (PPFD in $\mu mol\ m^{-2}\ s^{-1}$) from SW_{net24} (in $W\ m^{-2}$)

$$PPFD_{24} = 0.5 * SW_{net24}/(0.217 * (1 - albedo)), \quad (7)$$

where the factor of 0.5 is the fraction of the SW spectrum in the photosynthetic band, and 0.217 J μmol^{-1} is the unit conversion. We specify a fixed albedo of 0.2, perhaps slightly high for forests, but other terms in the energy balance such as G have been neglected, so this partly compensates. The actual photosynthetic energy absorbed (APPFD) depends on LAI and was modeled as

$$APPFD_{24} = PPFD_{24} * (1 - EXP(-0.6 * LAI)) \quad (8)$$

with LAI = 3 for grassland and 5 for forest.

[14] We then compute the 24-hour mean photosynthetic uptake in $\mu mol\ m^{-2}\ s^{-1}$ from $APPFD_{24}$ using

$$PH\_fd_{24} = -APPFD_{24} * epsilon * fstress * ftemp, \quad (9)$$

where the light use efficiency coefficient (epsilon) incorporates the efficiency of conversion of photons captured to CO_2 uptake, as well as the observation that light use efficiency increases as the ratio of direct to diffuse PPFD decreases.

$$epsilon = E_{veg} * PPFD_{24}^{-0.8501} \quad (10)$$

with E_{veg} = 6 for forest (obtained by a fit to data) and 10 for grassland, to represent their inherently different light use efficiencies. A quadratic soil moisture stress term (fstress), which is zero at a permanent wilting point of 0.137 and unity at 0.361, is defined as a function of fractional soil water content (SWC)

$$fstress = -1.4694 + 13.1 * SWC - 17.341 * SWC^2. \quad (11)$$

A quadratic temperature stress term (ftemp), which is zero at 0°C and has a maximum at 26°C, is defined as a function of surface temperature, T_{sf} (units, °C)

$$ftemp = 0.0749 * T_{sf} - 0.0014 * T_{sf}^2. \quad (12)$$

2.4. Respiration

[15] The 24-hour gross respiration is parameterized, using the same soil water stress function, as

$$RESP\_fd_{24} = fstress * \left[3.2 * Q_{10}^{0.1 * (Tsf-10)}\right], \quad (13)$$

where 3.2 is the observed ecosystem respiration rate ($\mu mol\ m^{-2}\ s^{-1}$) at 10°C and Q_{10} is the coefficient by which ecosystem respiration increases with temperature. The Q_{10} function (in brackets) is a basic kinetic function which accounts for the increase in molecular velocity (and hence respiration substrate velocity) as temperature increases by 10°C. A Q_{10} of 2 would represent a doubling of the respiration rate for a 10°C increase in temperature [*Salisbury and Ross*, 1992]. We used Q_{10} = 1.9 for forest and 2.2 for grassland. Table 1 summarizes the three vegetation parameters used to represent the two idealized ecosystems.

2.5. Net Ecosystem Exchange

[16] Plant physiologists, and more recently some micrometeorologists, have adopted the use of flux density as opposed to velocity to describe trace gas fluxes. Flux densities are more desirable than velocities, because a calculated flux density is independent of pressure and

changes considerably less with temperature as compared to a calculated velocity. Hence, flux densities are more immediately comparable across sites and experimental conditions. However, velocities are more easily translated into one-dimensional calculations where all parameters (e.g., pressure) are prescribed and trace-gas flux can be expressed as a change in mixing ratio per unit time. We convert both photosynthesis and respiration to units of velocity (ppm CO_2 m s^{-1}) from flux density (μmol CO_2 m^{-2} s^{-1}) using the molar density conversion

$$\rho_{mol} = P_{sf}/(8.314 * (T_{sf} + 273.15)), \quad (14)$$

where P_{sf} is the surface pressure in Pa, and 8.314 is the gas constant in J mol^{-1} K^{-1}

$$PH\_vel_{24} = PH\_fd_{24}/\rho_{mol} \quad (15a)$$

$$RESP\_vel_{24} = RESP\_fd_{24}/\rho_{mol}. \quad (15b)$$

The net ecosystem exchange, which represents the diurnally averaged flux of CO_2 at the surface in the ML CO_2 budget is just the sum

$$NEE = PH\_vel_{24} + RESP\_vel_{24}. \quad (16)$$

2.6. Stomatal Resistance

[17] We compute leaf stomatal resistance from the photosynthetic flux and the substomatal-to-ambient CO_2 gradient

$$R_{veg24} = (CO_{2I} - CO_{2L})/(1.5\,PH\_vel_{24}), \quad (17)$$

where the factor of 1.5 is the ratio of molecular diffusivities of H_2O to CO_2 (water diffuses faster than CO_2, so the effective resistance is less), and CO_{2I}, CO_{2L} are the CO_2 mixing ratios inside and outside the leaf. CO_{2L} will be computed from CO_{2m} in the mixed layer using an aerodynamic resistance at the surface, and CO_{2I} can be modeled as

$$CO_{2I} = CO_{2L} * C_{RH}, \quad (18)$$

where

$$C_{RH} = 0.5833 + 0.1667 * RH_{sf} \quad (19)$$

is a function of the surface relative humidity. This relationship is based on the Ball-Berry model of stomatal resistance where CO_{2I} is linearly related to leaf surface relative humidity (assumed to be equal to surface relative humidity here [*Ball*, 1987]). In general, there is an interplay between the rate of CO_2 diffusion into a leaf and the biochemical assimilation rate of CO_2. As relative humidity increases, stomatal resistance decreases, and as a result CO_{2I} increases due to higher rates of diffusion into the leaf relative to the rate of biochemical uptake. The rate of biochemical uptake is assumed to always be greater than the rate of diffusion through wide-open stomata, such that at 100% relative humidity CO_{2I} is still less than CO_{2L}. This gives

$$R_{veg24} = CO_{2L}(1 - C_{RH})/(1.5\,PH\_vel_{24}). \quad (20)$$

This photosynthetically determined stomatal resistance is then used to compute surface evaporation. We make the simplification that evaporation is entirely controlled by photosynthesis, which includes the approximation that there is no evaporation at night.

2.7. Method of Solution at Surface

[18] With R_{veg} given by (20), the equilibrium model of *Betts* [2000] is then solved by iteration. At the surface, we specify a range of SW_{net24} (or couple it to cloud mass flux, using (44a): see section 2.14, later) and find R_{net24} using (6c) to give LW_{net24}. We also specify soil moisture over a range, 0.16 to 0.32. This is the major factor controlling R_{veg} (see later). The aerodynamic resistance and surface pressure are specified, and the surface temperature (needed in (12), (13), and (14)) is found that satisfies the surface energy balance, (4), as in *Monteith* [1981], using the following surface transfer equations:

$$H_{24} = \rho_{sf} C_p g_a (T_{sf} - T_m), \quad (21a)$$

where ρ_{sf} is the surface air density, C_p is the specific heat, and g_a is an aerodynamic conductance, which will be specified. T_m is the temperature at the base of the ML, which we shall find from the mixed layer potential temperature, θ_m, using the Poisson equation

$$T_m = \theta_m (P_{sf}/100000)^{0.286},$$

where P_{sf} is the surface pressure. The evaporation

$$E_{24} = \rho_{sf}\{g_a g_v/(g_a + g_v)\}(q_s(T_{sf}) - q_m) \quad (21b)$$

involves $q_s(T_{sf})$, the saturation mixing ratio at T_{sf}, as well the additional conductance across the leaf, which is the inverse of the resistance

$$g_v = 1/R_{veg}.$$

ML mixing ratio, q_m, is linked back to T_m and relative humidity RH_m at the base of the ML, using equations in Appendix A, which are discussed later. For CO_2, we need to link the value outside the leaf to the mixed layer value

$$NEE_{24} = g_a(CO_{2L} - CO_{2m}). \quad (21c)$$

For radon, we shall specify a constant surface flux. Mixed layer values, θ_m, q_m, CO_{2m}, as well as their values above the ML, are discussed in the next section, as they involve the cloud layer and its coupling to the free troposphere.

2.8. ML Equilibrium

[19] We consider a well-mixed layer with potential temperature, θ_m, mixing ratio, q_m, CO_{2m}, and radon mixing ratio, Rn_m (see Figure 1), with jumps at ML top to

corresponding values just above cloud base in the shallow cloud layer

$$\Delta\theta_b = \theta_{cld} - \theta_m \tag{22a}$$

$$\Delta q_b = q_{cld} - q_m \tag{22b}$$

$$\Delta CO_{2b} = CO_{2cld} - CO_{2m} \tag{22c}$$

$$\Delta Rn_b = Rn_{cld} - Rn_m. \tag{22d}$$

Following *Betts* [2000], ML top is specified as cloud base, the lifting condensation level (LCL) of ML air with properties (θ_m, q_m), so that ML depth, h is given by

$$h = h_{LCL}(\theta_m, q_m, P_{sf}). \tag{23}$$

This subtle closure will be justified, when we solve the coupled system for the mass flux out of the ML (see section 2.12 and Figure 7b, later). At cloud base (suffix b), we couple the fluxes with a mass flux exchange, $\rho_b W_b$ [*Betts*, 1975]: the product of a cloud base velocity, W_b, and the density of dry air at the base of the cloud layer. Note that the specification of ML top as cloud base fundamentally changes the equilibrium surface energy balance by introducing one component of the coupling to the cloud field. (We shall introduce a second radiative component later in section 2.14.) In contrast, traditional analyses of equilibrium evaporation (see reviews by *Raupach* [2000, 2001]) are essentially dry models, which do not include these direct impacts of the lifting condensation level. The interpretation of an ''equilibrium'' cloud base in terms of real data, which will show the strong daytime diurnal cycle, with uncoupling of the stable BL at night is not straight forward. However, we will put aside these difficulties, in order to explore the idealized solutions. *Betts* [2004] does provide some justification for this by showing that the climate coupling over land can be described in terms of the 24-hour mean states of the boundary layer.

[20] The mixed layer equilibrium for q and CO_2 are just the balance of the surface and cloud base fluxes.

$$E_{24} = -\rho_b W_b \Delta q_b = E_b \tag{24a}$$

$$\rho_{sf} NEE = -\rho_b W_b \Delta CO_{2b}. \tag{24b}$$

If the dry air densities are both converted to molar densities by multiplying by the constant factor (1000/28.97), related to the conversion from Kg to g, and the molecular weight of dry air, we retrieve the CO_2 flux density in μmol CO_2 m^{-2} s^{-1}.

[21] The heat balance contains an additional term for the net radiative cooling of the ML, $(d\theta/dt)_{rad}$, which we specify as an external parameter (or couple to the cloud mass flux: see section 2.14 later).

$$\alpha_{sf} H_{24} = -\rho_b W_b \Delta\theta_b - \rho h_{LCL} (d\theta/dt)_{rad}, \tag{24c}$$

where h_{LCL} is the depth of the subcloud layer (with mean density ρ), and $\alpha_{sf} = (\theta/T)_{sf}$ is approximately unity, unless the surface pressure is far from 1000 hPa. It is convenient to rewrite (24c) as

$$\alpha_{sf} H_{24} = -\rho_b W_b \Delta\theta_b + F_{rad}, \tag{25}$$

where the radiative flux divergence across the ML is defined positive as

$$F_{rad} = -\rho\, h_{LCL} (d\theta/dt)_{rad} = (P_{LCL}/g)(d\theta/dt)_{rad}. \tag{26}$$

It is also convenient to define the pressure height of cloud base

$$P_{LCL} = \rho g\, h_{LCL}. \tag{27}$$

The relative humidity at the base of the ML is related to the LCL, so that it can be computed from P_{LCL}. Appendix A summarizes the general relationship between RH and P_{LCL}, which we use in the model solution. To solve the ML equilibrium, we use the inverse relationship to give RH_m at the base of the ML (equation (A3)), and from this find q_m using (A4) and T_m.

2.9. Upper Boundary Conditions for ML

[22] Closing the ML equations requires values for θ_{cld}, q_{cld}, CO_{2cld} and Rn_{cld} just above cloud base as a function of ML depth and the stratification above. As in *Betts* [2000], we do not solve for the thermodynamic structure in the cloud layer, but make two simplifications. We define

$$\theta_{cld} = 296 + \Gamma(P_{LCL} - 60), \tag{28}$$

where $\Gamma = -d\theta/dp$ is a measure of the stratification in the cloud layer. The 296 K sets the mean temperature of the model system. We find q_{cld} by constraining the subsaturation or RH_{cld} just above cloud base (shallow cumulus layers are characterized by having nearly constant subsaturation below their capping inversion), again using the relation between LCL and RH, shown in Appendix A. *Betts* [2000] simply specified a range, but to reduce the number of free parameters, here we shall couple subsaturation in the cloud layer (P_{LCLcld} and RH_{cld}) back to the ML pressure depth using an empirical relation

$$P_{LCLcld} = 50 + 0.3(P_{LCL} - 60). \tag{29}$$

Figure 3 shows that this relation constrains cloud layer RH_{cld} to decrease from 72% to 37% as the depth of the subcloud layer increases from 100 to 300 hPa (roughly 1000 to 3000 m), that is, as the ML gets deeper and drier. Equations (28) and (29) are simplifications which replace the more difficult task of solving for the coupled thermodynamic structure in the cloud layer, which includes the solution for the radiation field in a partially cloudy CBL (recall that in (24c) we specify the radiative term).

2.10. Radon Submodel

[23] Radon is produced in the soil from decay of radium at a constant rate and the rate of emission from the soil is approximately constant. Radon decays with a half-life of

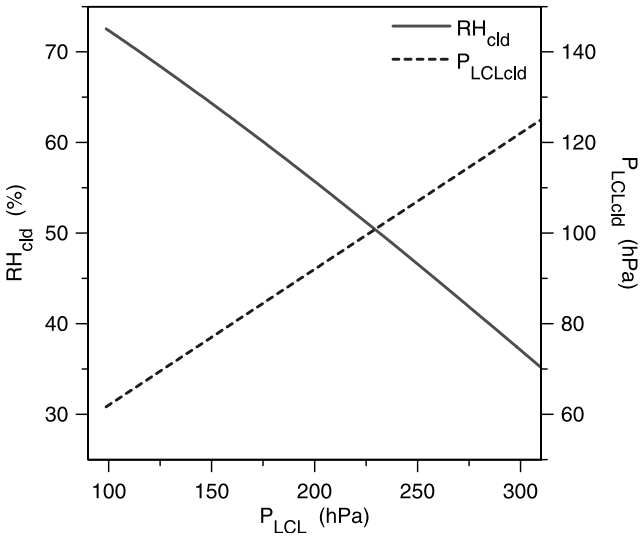

Figure 3. Closure for relative humidity above cloud base, and corresponding pressure height to lifting condensation level for air just above cloud base as a function of ML depth (in pressure thickness). See color version of this figure in the HTML.

3.8 days, so the ML equilibrium for radon contains an important decay term. Equilibrium radon in the ML can be written as,

$$F_{Rn} = -\rho_b W_b \Delta Rn_b + Rn_m * \rho W_{dm}, \qquad (29')$$

where F_{Rn} is the surface flux of radon, and W_{dm} represents the radon decay velocity scale for the ML, given by

$$\rho W_{dm} = \rho h_{LCL} * L_d, \qquad (30)$$

where L_d is the decay constant for radon, 2.089×10^{-6} s^{-1}. Using (26), replaces h_{LCL} in (27) with the pressure thickness

$$\rho W_{dm} = (P_{LCL}/g) * L_d \qquad (30')$$

For our analysis we used a constant F_{Rn} of 0.021 Bq m^{-2} s^{-1}. Typical concentrations of radon are about 0.4 Bq m^3 at STP (standard temperature and pressure) in the free troposphere, and 1.8–3.7 Bq m^3 in the ML [*Kritz et al.*, 1998].

[24] CO_2 and radon are transported out of the subcloud layer into clouds, and then mixed through the cloud layer, but they can be considered passive tracers during this process (except for the radon decay). We shall solve for the cloud base mass flux using (24a), but we need a further closure to give values for CO_{2cld} and Rn_{cld} in (22c) and (22d). For this we consider the equilibrium of the CBL as a whole.

2.11. CBL Equilibrium

[25] The condensation, upward advection, and evaporation of liquid water in shallow cumulus clouds are a destabilizing process [*Betts*, 1973, 1975], and the CBL will deepen, entraining warm dry air from above, unless there is a compensating subsidence. In the subsiding branches of the atmospheric circulation, such as the trade winds over the oceans, the radiatively driven subsidence, which is of order 0.005 m s^{-1} or 0.05 Pa s^{-1}, balance the CBL growth by entrainment [*Betts and Ridgway*, 1988, 1989]. Suppose such an equilibrium is also established in the long-term over land with subsidence balancing an entrainment velocity, W_E. If we suppose there is constant subsidence in the cloud layer (that is, all the mass divergence is in the ML), the equilibrium CO_2 budget for the whole CBL is just

$$\rho_{sf}\, NEE = -\rho_b\, W_{Eb}(CO_{2t} - CO_{2m}), \qquad (31)$$

where CO_{2t} is the value in the "free troposphere," which we shall consider fixed at 365 ppm. We have again defined a mass flux at cloud base corresponding to the subsidence, which being constant above cloud base, satisfies

$$\rho_b\, W_{Eb} = \rho_t\, W_{Et}. \qquad (32)$$

Following conventional meteorological practice, we shall solve the system in pressure coordinates to absorb the density variation with height. Equation (31) gives a direct solution for CO_{2m}, as a balance between the surface NEE and the free tropospheric entrainment, given the vertical mass flux $\rho_b\, W_{Eb}$. The equivalent equilibrium equation for mixing ratio is

$$E_{24} = -\rho_b\, W_{Eb}(q_t - q_m), \qquad (33)$$

where q_t is a "free tropospheric" mixing ratio, above the CBL, typically in the range 1 to 4 g Kg^{-1}. This can then be inverted to give the mass exchange

$$\rho_b W_{Eb} = E_{24}/(q_m - q_t). \qquad (33')$$

Equations (24a) and (33) can both be satisfied. We use (24a) to determine the total cloud base mass exchange as part of a fully coupled ML equilibrium, and then (33) to diagnose the smaller subsidence or mass exchange needed to maintain the CBL equilibrium. A little manipulation shows that the values above cloud base satisfy

$$q_{Cld} = q_t + E_{24} * \rho_b\, W_{CLD}/(\rho_b\, W_b * \rho_b W_{Eb}) \qquad (34a)$$

$$CO_{2Cld} = CO_{2t} + \rho_{sf}\, NEE * \rho_b\, W_{CLD}/(\rho_b\, W_b * \rho_b W_{Eb}), \qquad (34b)$$

where we have defined a net cloud mass flux

$$\rho_b W_{CLD} = \rho_b W_b - \rho_b W_{Eb} \qquad (35)$$

as a measure of an additional "cloud" mass exchange needed to pump sufficient water vapor out of the ML to satisfy the ML component of the equilibrium model. Equations (34a) and (34b) show that $q_{cld} > q_t$ and $CO_{2cld} > CO_{2t}$, provided $W_{CLD} > 0$. The extra cloud flux modifies the layer above cloud base, and balances the mean subsidence in this same layer. We shall find that if evaporation is very low, so that the ML becomes very deep, then W_{CLD} goes to zero, and the conceptual cloud field disappears (see section 3.2), and unmodified "free tropospheric" air is entrained into the ML.

Table 2. Parameter Ranges Used for Model Solutions

Parameter	Range	Default: Units
Aerodynamic conductance: g_a		0.025: m s^{-1}
Entrainment parameter: k		0.2
Soil water content: SWC	0.15 to 0.35	
Net shortwave: SW_{net}	150 to 250[a]	200: W m^{-2}
Stratification above ML: Γ	0.04 to 0.07	0.06: K hPa^{-1}
Humidity above ML: RH_{cld}	modeled	
BL radiative cooling rate	−2 to −3[a]	−2.5: K day^{-1}
CO_{2t} above CBL		365: ppm
q_t above CBL	1 to 4	3: g Kg^{-1}

[a]Cloud-coupled solutions given by equations (45a) and (45b) were also used.

[26] The radon balance is more complex as there are the additional decay terms. The equilibrium radon budget for the whole CBL is

$$F_{Rn} = -\rho_b W_{Eb} \Delta Rn_b + Rn_m * \rho W_{dm} + Rn_{CL} * \rho_{CL} W_{dCL}, \quad (36)$$

where the decay constant for the cloud layer (subscript CL) can be written

$$\rho_{CL} W_{dCL} = (P_{CL}/g) * L_d. \quad (37)$$

However, two additional assumptions are needed to compute the decay in the cloud layer. One is cloud layer depth, for which we simply assume the entire CBL is 350hPa deep, so that the cloud layer shrinks as the ML deepens, and $P_{CL} = 350 - P_{LCL}$. The second is that, unlike the ML, the cloud layer is generally not well mixed, so we assume a linear distribution between the value just above cloud base and the free troposphere, so that $Rn_{CL} = (Rn_{Cld} + Rn_t)/2$. Algebraic manipulation then gives these expressions for radon just above cloud base and for the ML

$$Rn_{Cld} = [Rn_t(1 + C1)(1 - C3) + F_{Rn}\rho_b W_{CLD} / (\rho_b W_b * \rho_b W_{Eb})]/[1 + C2 + C3 + C1C3] \quad (38a)$$

$$Rn_m = [Rn_t(1 - C3) + F_{Rn}(\rho_b W_b + \rho_b W_{Eb} * (C2 + C3 + C1C3) / (\rho_b W_b * \rho_b W_{Eb} * (1 + C1))]/[1 + C2 + C3 + C1C3], \quad (38b)$$

where we have defined the ratios $C1 = \rho W_{dm}/\rho_b W_b$; $C2 = \rho W_{dm}/\rho_b W_{Eb}$; $C3 = \rho_{CL} W_{dCL}/\rho_b W_{Eb}$. For almost all ML solutions, C1, C2 and C3 are <1. Note that because of the additional decay in the cloud layer, (38a) does not give $Rnc_{ld} = Rn_t$, when $\rho_b W_{CLD} = 0$. This would require a refinement to the model to ensure that P_{CL} and therefore C3 also become zero. However, the impact of our constant CBL depth assumption of Rn_m is small.

2.12. Coupling of Transports in CBL

[27] For an equilibrium CBL, (31) and (33) link the surface NEE and E to a common mass transport and a gradient between the ML and the free troposphere. Dividing (31) by (33) gives

$$\rho_{sf} NEE/E_{24} = (CO_{2t} - CO_{2m})/(q_t - q_m). \quad (39)$$

In a companion paper, *Helliker et al.* [2004] use (39) to estimate NEE over the annual cycle from measurements of surface evaporation and the vertical gradients of CO_2 and q between the ML and midtroposphere.

2.13. Closure and Method of Solution

[28] As in *Betts* [2000] (based on the earlier papers of *Betts* [1973] and *Tennekes* [1973]), we use a ML closure on the virtual potential heat flux

$$H_{vb} = -k H_{vsf} \text{ with } k = 0.2, \quad (40)$$

where the virtual potential heat flux can be approximated as

$$H_v = \alpha H + 0.075 \lambda E. \quad (41)$$

The coefficient is $0.608\,\theta\,(C_p/\lambda) = 0.075$ at $\theta = 302$ K, and it will be treated as a constant. Substituting (24a) and (25) in (40) and rearranging gives

$$H_{vb} = -k F_{rad}/(k + 1). \quad (42)$$

Since $\alpha_b H_b = H_{vb} - 0.073\,\lambda E_b$, we can, using (42), (25), (24a), and (4), solve for

$$\alpha_b H_b = -\rho_b W_b \Delta\theta_b = [-k F_{rad}/(k + 1) - 0.075(R_{net24} - F_{rad})]/(1 - 0.073). \quad (43)$$

This form of the solution is useful because it does not depend on the surface energy flux partition. The similar solution for the surface heat flux is

$$\alpha_{sf} H_{24} = [F_{rad}/(k + 1) - 0.075 R_{net_{24}}]/(1 - 0.075). \quad (44)$$

Since F_{rad} is proportional to ML depth, h_{LCL}, from (26), equation (44) determines the surface sensible heat flux as a linear function of $P_{LCL} = \rho\, g\, H_{LCL}$, as long as the ML radiative cooling rate is a constant. The surface heat flux is primarily controlled by the depth of the ML and its radiative cooling rate [*Betts*, 2000]. In fact, all the fluxes at both top and bottom of the ML are then linear functions of P_{LCL}, so we shall use this as a coordinate in many figures.

[29] Table 2 shows the set of specified external parameters, their default values and the ranges used, if they were varied. We find equilibrium solutions iteratively. Starting with a guess of P_{LCL}, we find θ_{cld} and P_{LCLcld} from (28) and (29), which also gives us q_{cld}. A first guess of $\Delta\theta_b$ gives θ_m, and q_m is found from RH_m at the base of the ML, as it is a unique function of P_{LCL} (see equation (A3)). From θ_m and q_m, we can find a T_{sf} that gives an H and λE that satisfy (4), with R_{veg} given by (20). An iteration is needed on R_{veg}, since it is a weak function of T_{sf} and RH_{sf}. Then P_{LCL} can be updated from (44) using (26). $\Delta\theta_b$ can be updated from (43) by finding $\rho_b W_b$ from (24a) and (22b). Solutions for the CO_2 structure follow from (33'), (31), and (24b). CO_{2m} has a weak impact on R_{veg}. Solutions for radon then follow from (38).

2.14. Cloud-Coupled Solutions

[30] The formation of clouds at the top of the ML introduces two feedbacks. ML top is constrained to the

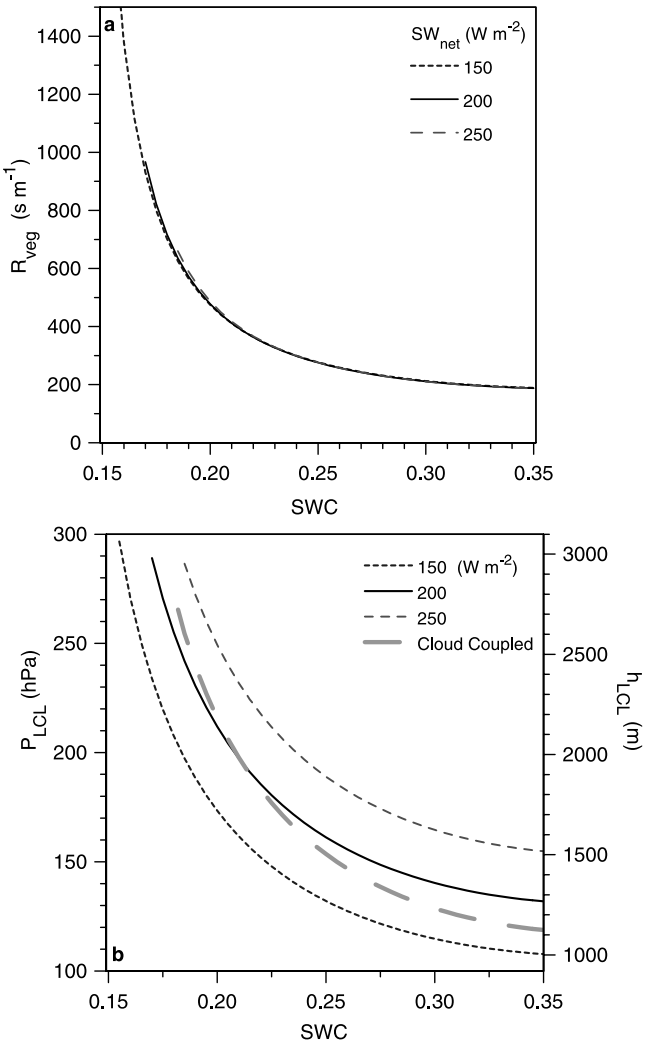

Figure 4. (a) Vegetative resistance as a function of soil water content and net short-wave. (b) Corresponding ML depth in pressure and height coordinates: cloud-coupled solution is shown as heavy dashes. See color version of this figure in the HTML.

LCL, as represented by (23), and the cloud field has a radiative impact. For two variables, surface net short-wave and ML radiative cooling rate, which both depend on cloud-cover, in addition to using parameter ranges in Table 2, we also defined "cloud-coupled" values, using these simple closures related to the net cloud mass flux, given by (35).

$$SW_{net} = 250 - 100\rho_b W_{CLD}/0.01 \text{ for } \rho_b W_{CLD} > 0; \text{ and } 250 \text{ for } \rho_b W_{CLD} < 0 \quad (45a)$$

$$(d\theta/dt)_{rad} = -3 + \rho_b W_{CLD}/0.01 \text{ for } \rho_b W_{CLD} > 0; \text{ and } -3 \text{ for } \rho_b W_{CLD} < 0. \quad (45b)$$

In the range of solutions, $0 < \rho_b W_{CLD} < 0.01$, (44a) and (44b) give the same ranges shown in Table 2, namely, $250 > SW_{net} > 150$ Wm^{-2} and $-3 < (d\theta/dt)_{rad} < -2$ K day^{-1}, that is the net short-wave and ML cooling rate decrease as the cloud mass flux increases. Over the same range, the surface LW_{net24}, which satisfies (6c), increases from -80 to -40 Wm^{-2}. The range of daily net SW radiation that we present is consistent with undisturbed conditions in summer.

3. Equilibrium Solutions

[31] We shall show the sensitivity of the equilibrium solutions to the parameter ranges shown in Table 2 and in addition, some figures will also show the cloud-coupled solutions, using (45a) and (45b). Since all fluxes are 24-hour means, we will drop the suffix 24 in the figures.

3.1. Sensitivity to Soil Moisture and ML Depth

[32] This sensitivity is the strongest control on vegetative (stomatal) resistance, so we first show the equilibrium solutions with varying SWC for three values of SW_{net} (we could have shown R_{net} instead, since the SW and LW fluxes are coupled through (6c)), with the stratification, ML cooling rate and q_t set at their default values, shown in Table 2.

[33] Figure 4a shows that R_{veg} increases sharply, as SWC drops toward the model permanent wilting point of 0.137, since R_{veg} is affected by the stress function (fstress in (11)). Surprisingly, however, except at very low SWC, there is almost no dependence on SW_{net}. This arises from a cancellation of effects in (20). Photosynthesis increases with SW_{net}, but changes in CO_2 and RH_{sf} at the leaf largely compensate in (20). This simplification, which appears to be a characteristic of the Wisconsin forest data, leads to a reduced variability in the CO_2 budget in later figures. Figure 4b shows that the equilibrium ML depth increases sharply as SWC decreases (and stomatal resistance increases), as reduced evaporation leads to a warmer drier equilibrium ML; and also increases as the radiative driver, SW_{net}, increases the surface energy fluxes. The left-hand scale shows ML depth as a pressure thickness, which we shall use in subsequent figures; and the right-hand scale shows the corresponding depth to cloud base in meters (with slight approximation). The heavy dashed line is the single cloud-coupled solution, derived by making a further iteration to satisfy (45a) and (45b) as well.

[34] Figures 5a and 5c show the surface energy fluxes as a function of SWC (left) and P_{LCL} (right). Figures 5b and 5d show the corresponding daily mean evaporative fraction, defined as

$$EF = \lambda E/(H + \lambda E). \quad (46)$$

We shall discuss the family of fixed SW_{net} curves first. As expected, Figure 5a shows that for fixed SW_{net} evaporation increases and sensible heat flux decreases nonlinearly as SWC increases, since R_{veg} decreases (Figure 4a), while both fluxes increase as the surface radiative forcing SW_{net} increases. Figure 5b shows that the increase of EF with SWC is almost independent of SW_{net} (this follows from the very weak dependence of R_{veg} on SW_{net} in Figure 4a). Figure 4c shows that the surface fluxes are linear functions of ML pressure thickness as discussed in section 2.13. As SW_{net} increases (and R_{net} with it using (6c)), evaporation increases, but the surface sensible heat flux changes little, as (44) shows it depends primarily on F_{rad}. Consequently, for a given ML depth, EF increases with surface radiative forcing

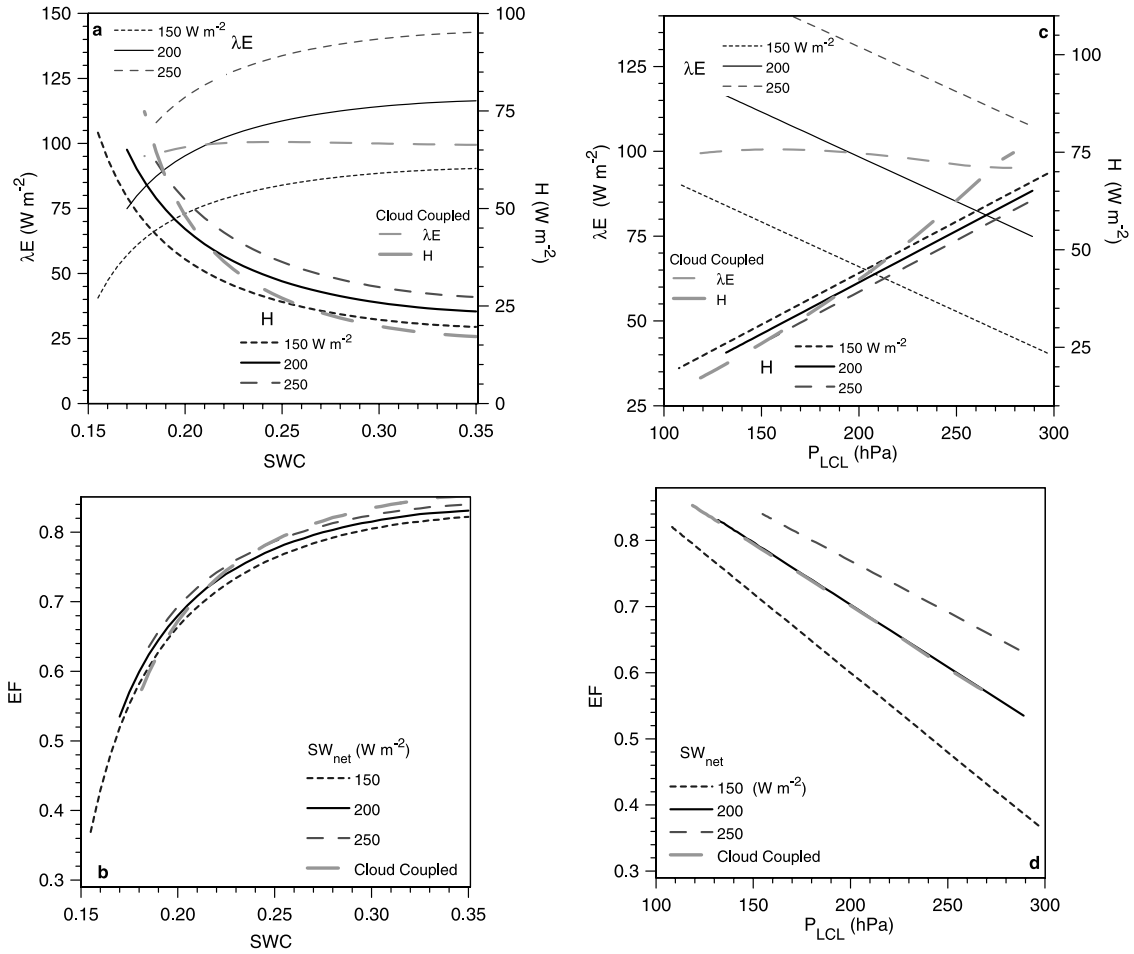

Figure 5. (a) Surface evaporation and sensible heat flux as a function of soil water content and net short-wave. (b) As in Figure 5a for evaporative fraction. (c) As in Figure 5a as a function of ML pressure thickness. (d) As in Figure 5b as a function of ML pressure thickness. See color version of this figure in the HTML.

(Figure 5d). Note that the left and right panels give quite a different perspective on the surface energy balance. As a function of soil water, the fluxes are nonlinear, but EF is only a weak function of SW_{net}. As a function of ML depth, the fluxes become linear, because the energy balance terms are proportional to depth. However, whereas at a given SWC, H increases with SW_{net}, for a given ML depth, H decreases slightly with SW_{net}, because of the large increase of equilibrium depth with solar forcing, shown in Figure 4b.

[35] The upper panels show that our cloud-coupled model (heavy dashes) has a significant impact on the fluxes. H becomes nonlinear, primarily because the ML radiative cooling rate increases from wet to dry soils (the corresponding cloud mass flux will be shown later in Figure 8b); while the latent heat flux has very little variation, as R_{net} increases significantly from wet to dry soils from (45a) and (6c). However, the lower panels show that the corresponding impact on EF is rather small.

[36] Figure 6 shows the corresponding set of plots as a function of SWC on the left and P_{LCL} on the right for θ_m and q_m (upper panels) and CO_{2m} and radon (lower panels). The cloud-coupled solutions, shown in Figures 6a, 6b, and 6d, intersect the family of fixed SW_{net} solutions because of the variation of SW_{net} given by (45a). The cloud-coupled solutions for Figure 6c are indistinguishable from the plots for SW_{net} = 200 W m^{-2}, and are not shown. We see, as expected, that the ML gets warmer and drier as SWC decreases and the ML deepens. As a function of SWC (Figure 6a), θ_m and q_m also get warmer and drier with SW_{net}. However, when plotted as a function of P_{LCL} (Figure 6c), the ML gets slightly warmer and wetter as the surface SW_{net} increases, as discussed in *Betts* [2000]. In terms of the model, equations (28) and (29) determine θ_{cld}, q_{cld} just above the ML from P_{LCL}. The jump $\Delta\theta$ at cloud base decreases slightly as the cloud base mass flux increases with SW_{net} (see section 3.2), so that θ_m increases slightly. In the moisture budget, the λE increases faster with SW_{net} than the cloud base mass flux, so that the jump Δq at cloud base increases in magnitude, and so q_m increases.

[37] Figures 6b and 6d show the corresponding plots for ML CO_2 and radon. For radon, where the surface flux is constant, the ML equilibrium depends strongly on the radiative forcing, since this affects the cloud base flux (see next section), so Rn_m decreases in both Figures 6b and 6d as SW_{net} increases. For CO_{2m}, the decrease with increasing SWC or decreasing ML depth at constant SW_{net} follows from the increasing photosynthesis as fstress in (11) approaches unity. As a function of SWC, NEE depends

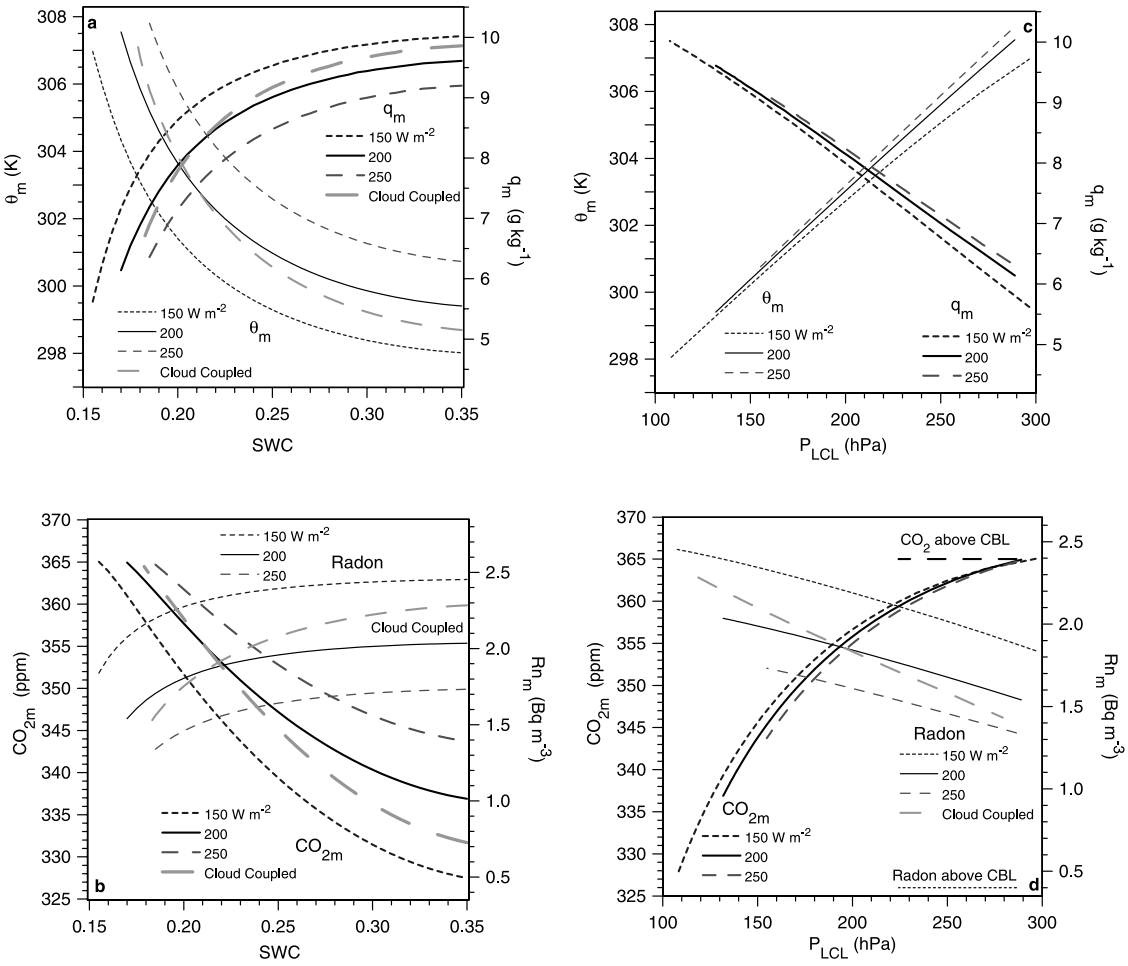

Figure 6. (a) Dependence of equilibrium ML potential temperature and mixing ratio on SWC and net shortwave. (b) As in Figure 6a for ML CO_2 and radon. (c) As in Figure 6a as a function of ML pressure depth. (d) As in Figure 6b as a function of ML pressure depth. See color version of this figure in the HTML.

rather weakly on SW_{net} (see Figure 7a), so that CO_{2m} increases with SW_{net}, as the cloud base mass flux increases, transporting more (low) CO_2 out of the ML. However, as with q_m, as a function of P_{LCL}, we see the reverse; CO_{2m} decreases weakly with increasing surface solar forcing.

[38] Figure 7a shows the increase of both photosynthesis and respiration with increasing SWC and SW_{net}. The difference between the two curves is the NEE, which increases over wetter soils, but has rather a weak dependence on SW_{net}, except over dry soil, when NEE is reduced. This insensitivity of NEE to SW_{net} is again related to the very weak dependence of R_{veg} on SW_{net} shown in Figure 4a. This, in turn, leads to the tight coupling between ML CO_{2m} and q_m shown on the left-hand scale of Figure 7b, which is almost insensitive to net shortwave (as can be deduced from Figures 6c and 6d). However, the link between NEE and CO_{2m}, shown on the right-hand scale, is strongly dependent on SW_{net} because CO_{2m} is directly coupled to the vertical exchange, shown in the next section. The cloud-coupled equilibrium solution is more nonlinear.

3.2. Vertical Mass Fluxes

[39] As part of the solution, we determine two equilibrium mass fluxes: the mass exchange, $\rho_b W_b$, at the top of the mixed layer which balances the surface fluxes in (24); and the mass exchange, $\rho_b W_{Eb}$, with the free troposphere above the CBL, which balances the surface fluxes in (31) and (33). These are both shown in Figure 8a as a function of SW_{net}, and for the cloud-coupled solution. For the specified SW_{net} family, the mass exchange, $\rho_b W_{Eb}$, with the free troposphere needed to give CBL equilibrium, increases weakly with ML depth, and sharply with SW_{net}. The mass exchange, $\rho_b W_b$, which balances the ML budgets also increases with SW_{net}, but falls steeply as the ML deepens, so that each pair crosses near a ML depth of 280 hPa. (This exact value of course depends on many internal parameters of the model, as well as the specified external boundary conditions.) The heavy dashed curves show the cloud-coupled solutions, which have a similar intersection, but cut across the family of SW_{net} curves. The difference between each pair of curves is the additional "cloud" mass flux, $\rho_b W_{CLD}$, defined in (35), and it is shown in Figure 8b. This cloud mass flux does increase with SW_{net}, but all the curves fall steeply as the ML deepens to cross zero at a depth near 280 hPa. Above this ML depth, the total mass exchange at cloud base is less than the equilibrium subsidence, and $q_{CLd} < q_t$, and the model with a cloudy boundary layer becomes physically unrealistic. Below 280 hPa, $\rho_b W_{CLD}$ is a measure of the extra "cloud" mass exchange needed to pump sufficient water vapor out of the ML to satisfy the ML component of the equilibrium

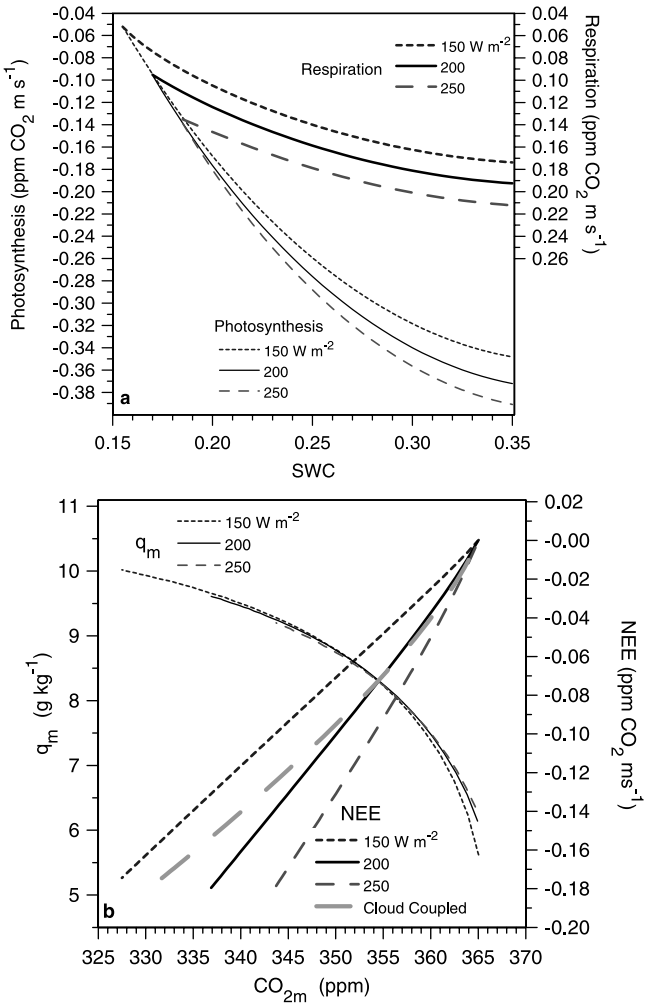

Figure 7. (a) Dependence of photosynthesis and respiration on SWC and SW_{net}. (b) Coupling between q_m and CO_{2m} (left-hand scale), and CO_{2m} and net ecosystem exchange (right-hand scale) as a function of net shortwave. See color version of this figure in the HTML.

model. Above this ML depth threshold, we could consider that the solutions to the dry ML model would be appropriate, without the condition that the top of the ML also be cloud base. The cloud-coupled solution is almost linear with ML depth, so that (45a) and (45b) also give almost a linear variation of SW_{net} and $(d\theta/dt)_{rad}$ with ML depth.

[40] One general and important conclusion is that unless SWC becomes very low so that the ML becomes very deep, the assumptions of the model can be satisfied, with cloud base at the top of the ML and a shallow cloud field above in balance with weak large-scale subsidence. For shallow MLs, much stronger subsidence (equal to $\rho_b W_b$ in Figure 8a) is needed to suppress the cloud field, and give a BL without clouds. We see from Figure 6d that ML radon concentrations are rather sensitive to the cloud base exchange, and therefore might be a useful way of estimating it, provided estimates of the surface radon flux are available.

3.3. Sensitivity to Mixing Ratio Above the CBL

[41] In the next three sections we shall select one parameter range from Table 2 and keep the others at their defaults. For brevity, we shall not show the cloud-coupled solutions because they give rather similar families of curves, which for the most part can be qualitatively inferred from the plots in the previous sections. The mixing ratio q_t of the "free troposphere" above the CBL has no direct effect on the energy balance of the ML or on its thermodynamic solutions for θ_m and q_m, but it does impact the mass flux $\rho_b W_{Eb}$ through (33). Figure 9a shows that while the cloud base exchange, $\rho_b W_b$, is constant (for default $SW_{net} = 200\ Wm^{-2}$: it has a small variation for the cloud-coupled solution, not shown), $\rho_b W_{Eb}$ derived from (33) increases with q_t, with the corresponding shift of the entire net cloud mass flux profile shown in Figure 9b. Essentially the ML stays the same, but a larger cloud mass flux compensates for the drier air entrained at CBL top. This change in $\rho_b W_{Eb}$ has a

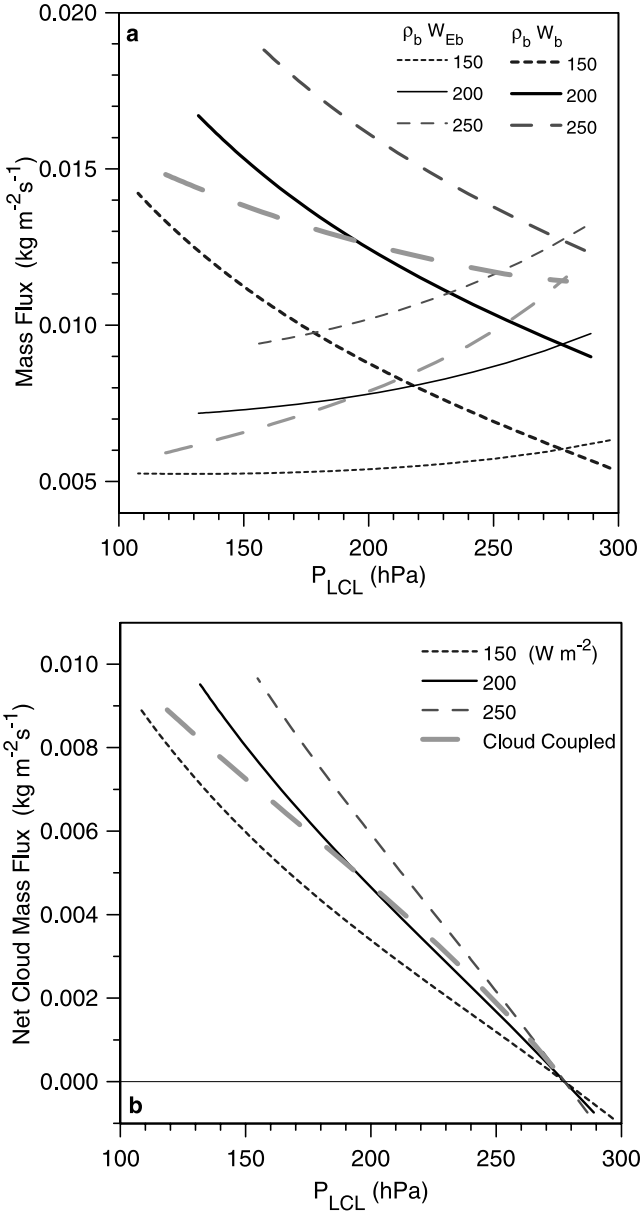

Figure 8. (a) Mass exchange at cloud base, and with free troposphere above CBL as a function of net short-wave. (b) Corresponding net cloud mass flux. See color version of this figure in the HTML.

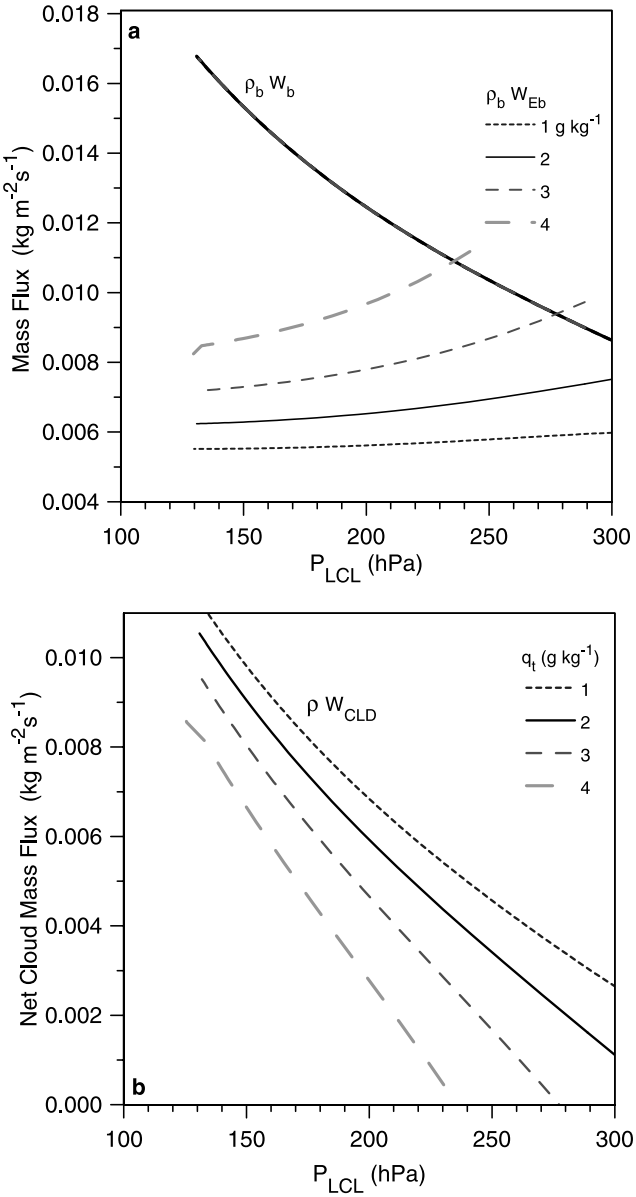

Figure 9. (a) As in Figure 8a as a function of q_t above the CBL. (b) Corresponding net cloud mass flux. See color version of this figure in the HTML.

corresponding impact on the ML equilibrium for CO_{2m} and radon, shown in Figure 10. As passive scalars, both move closer to their values in the "free troposphere" as the $\rho_b W_{Eb}$ increases. As shown in Figure 11, this affects the coupling between CO_{2m} and q_m, which is not affected by q_t; and between CO_{2m} and NEE, since NEE is almost unaffected by these changes in CO_{2m} (not shown). We can conclude, not surprisingly, that if we are to relate the moisture structure and fluxes to the CO_2 structure and NEE, we need to know both the mixing ratio and CO_2 content of air entrained into the CBL.

[42] A typical radiative equilibrium subsidence rate above the CBL at warm temperatures is 0.05 Pa s^{-1} [e.g., *Betts and Ridgway*, 1989], corresponding to a mass flux (dividing by 9.8 ms^{-2}) of 0.005 kg m^{-2} s^{-1} in Figures 8a and 9a, at the lower end of the range for $\rho_b W_{Eb}$, the mass exchange necessary to keep the CBL from moistening. In other words, a subsidence rate of $\rho_b W_{Eb}$ is needed to keep the CBL from growing deeper, given that the air being entrained into the CBL has mixing ratio q_t. Conversely, if the subsidence, whether radiatively or dynamically driven, is less then $\rho_b W_{Eb}$ in Figure 8a, then the CBL cannot be in equilibrium, and we could interpret the difference as a CBL growth rate. Such a growth rate would be small: for example, a growth of 0.02 Pa s^{-1} corresponds to only 20 hPa day^{-1}, so the ML equilibrium solutions could be quite well satisfied over timescales of several days. If the CBL does deepen beyond the middle troposphere, then the growth of precipitation particles, and their evaporation as they fall, will introduce additional processes that we have not considered in our simple model.

3.4. Sensitivity to Stability

[43] The stability parameter Γ controls potential temperature above cloud base, θ_{cld}, through (28) and also q_{cld}, since (29) determines RH_{cld}, as shown in Figure 3. We performed sensitivity studies to stability, but for brevity we do not show these figures. Increasing stability warms and moistens the ML significantly. The impact on CO_{2m} is relatively small, while ML radon increases, because the vertical mass exchanges are reduced as a partial compensation for the increases in q_m and q_{cld}. In the CO_2 budget, the drop in the mass exchange at the top of the ML is largely compensated by a fall in the NEE, primarily caused by warmer surface temperatures increasing respiration. As a function of ML depth, the surface H and λE are independent of Γ, but the warming of θ_m, and q_m changes the surface energy budget and NEE in relation to the SWC, which could be considered an independent surface variable. For the same SWC, P_{LCL} gets shallower as Γ increases, and EF increases. Essentially we found that warmer temperatures in the cloud layer (which may be linked to warmer temperatures in the middle troposphere) warm and moisten the ML, lower cloud base, increase evaporation and reduce the sensible heat flux and NEE. However, a better representation of the temperature structure of the CBL is needed,

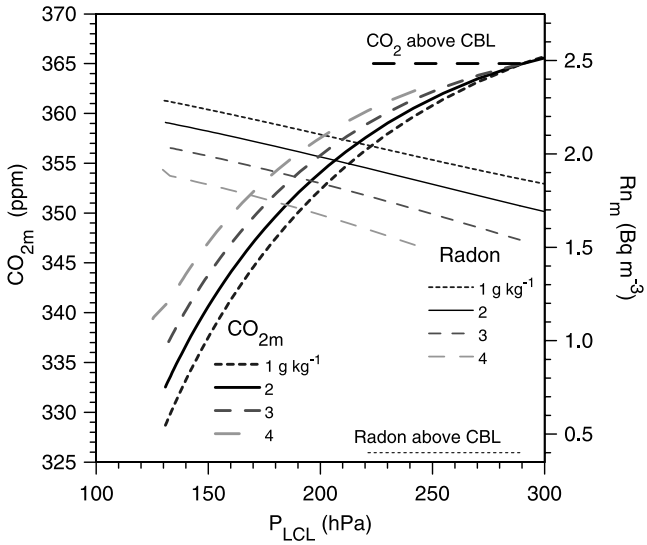

Figure 10. Dependence of ML CO_{2m} and radon on q_t above the CBL. See color version of this figure in the HTML.

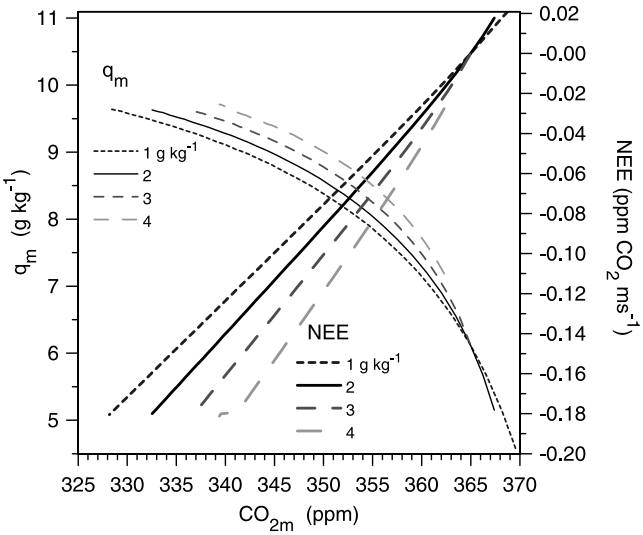

Figure 11. Coupling between q_m and CO_{2m} (left-hand scale), and CO_{2m} and NEE (right-hand scale) as exchange with free troposphere is influenced by q_t above the CBL. See color version of this figure in the HTML.

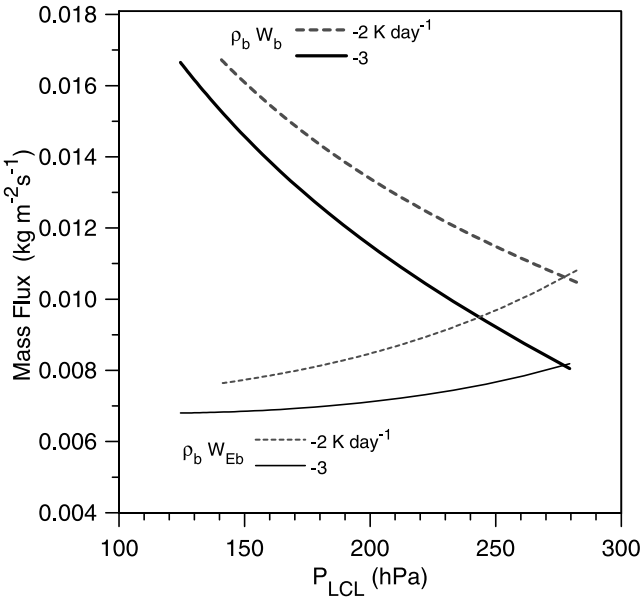

Figure 13. As in Figure 8a as a function of ML radiative cooling rate. See color version of this figure in the HTML.

rather than our simple specification of a stability parameter. This requires modeling the cloud layer with a coupled radiation code.

3.5. Sensitivity to ML Radiative Cooling Rate

[44] The ML radiative cooling rate and the ML depth control the surface sensible heat flux through (26) and (44). Figure 12 shows the impact on the equilibrium ML as a function of SWC, keeping fixed the other parameters in Table 2 (SW_{net} = 200 Wm^{-2}, q_t = 3 g kg^{-1}, Γ = 0.06 K hPa^{-1}). As the ML radiative cooling rate increases, the ML becomes cooler, H increases and λE decreases; and both ML depth and EF decrease. Figure 13 shows that the mass exchange terms, $\rho_b W_b$ and $\rho_b W_{Eb}$, both decrease, because of the decrease of evaporation. As a function of ML depth, Figure 14a shows that the ML actually gets cooler and drier as ML radiative cooling increases, while both CO_{2m} and radon increase (Figure 14b). The fall of ML depth with increased cooling shown in Figure 12 means that, as in Figure 6, as a function of SWC, CO_2 decreases, and q_m increases with ML radiative cooling (not shown). Figure 15 shows that while the coupling between CO_{2m} and NEE changes with ML radiative cooling (respiration decreases as the ML cools), that between CO_{2m} and q_m is almost unaffected. Comparison of Figures 12–15 with Figures 4–8 shows that the response of the ML equilibrium to increased surface radiative forcing from 200 to 250 Wm^{-2} is qualitatively similar to the response of reduced radiative cooling of the ML from −3 to −2 K day^{-1}, except for EF, where the impact of F_{rad} on H_{24} in (44) is large.

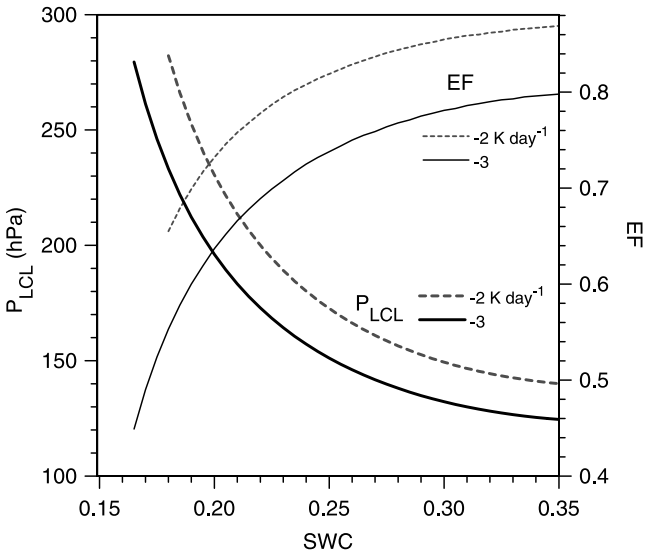

Figure 12. ML depth and evaporative fraction as a function of soil water and ML radiative cooling rate. See color version of this figure in the HTML.

3.6. Dependence on Vegetation Type

[45] We model two idealized ecosystems, forest and grassland, represented by the three different vegetation parameters given in Table 1. For grassland, both photosynthesis and respiration are greater for the same SWC, SW_{net} and surface temperature. Figure 16 shows that as a function of SWC (other parameters set at their defaults in Table 2), EF increases for grassland and ML depth decreases, both a direct response to increased photosynthesis, and reduced R_{veg}. Consequently as a function of SWC, for grassland, the ML is cooler, moister, and has lower CO_{2m} (not shown). However, as a function of ML depth, the picture again changes and simplifies, as in Figure 6. The ML θ_m, q_m, radon, all the mass fluxes and energy fluxes are independent of ecosystem: the lower grassland R_{veg} gives a lower equilibrium depth, but the thermodynamic structure and fluxes depend only on this depth. The cloud-coupled solutions corresponding to Figure 16 (not shown) are just slightly steeper (compare Figures 3b and 4b). Figure 17 shows that the coupling between CO_2 and NEE does not depends on ecosystem, while the coupling between CO_2 and q_m has only a weak dependence. The larger NEE over grassland, and the shallower equilibrium depth, however, extends the curves to

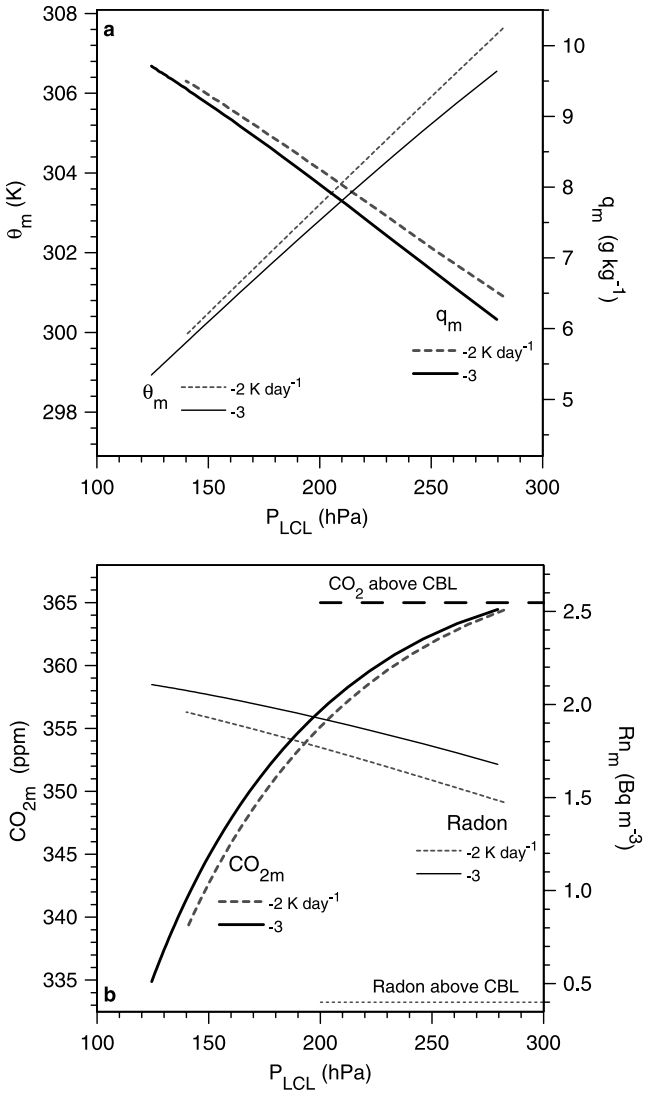

Figure 14. As in Figure 6, showing dependence on ML radiative cooling rate. See color version of this figure in the HTML.

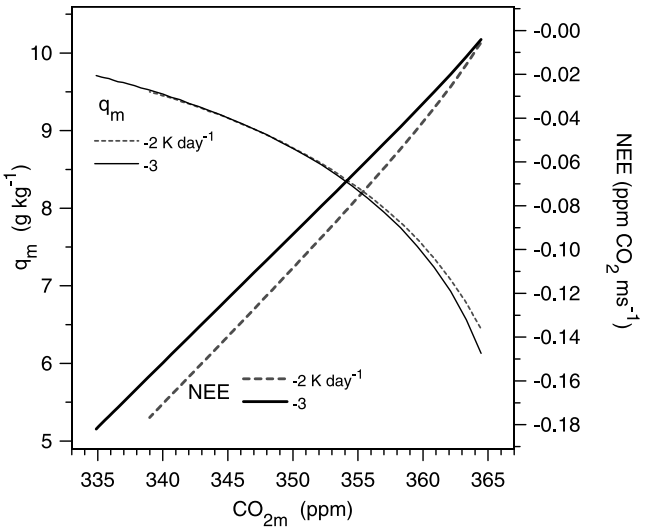

Figure 15. As in Figure 7b, showing dependence on ML radiative cooling rate. See color version of this figure in the HTML.

much lower equilibrium values of CO_2. This is clearly a useful result, since generally the landscape will have mixed ecosystems. In this final figure we show the cloud-coupled solutions for CO_2 and NEE. These extend to lower CO_2 values because of the lower SW_{net} and vertical mass exchanges over moist soils, and are more curved, because of the internal variation of SW_{net} (compare Figure 7), but the dependence on ecosystem is very weak.

4. Discussion and Conclusions

[46] This simple equilibrium model gives insight into the coupling between the surface energy and water budgets and net ecosystem exchange, and the mixed layer equilibrium of potential temperature, water vapor, CO_2 (and other tracers such as radon). Mixed layer parameters, such as θ_m, q_m, CO_{2m}, and Rn_m as well as ML depth (our P_{LCL} in pressure coordinates), are relatively easy parameters to measure, so we expect that the solutions could be used to help constrain surface flux estimates averaged over the diurnal cycle. We have shown solutions as a function of a set of external parameters: soil water content, which directly impacts respiration and photosynthesis, and hence transpiration; the surface net shortwave, directly linked here to net radiation, which is also coupled to photosynthesis and transpiration; and the radiative cooling of the ML, which in the equilibrium model directly affects the surface sensible heat flux. We also show ''cloud-coupled'' solutions which link two of these, surface net shortwave and the radiative cooling of the ML, back to the net cloud mass flux in the equilibrium model, as a simple representation of the impact of cloud cover. Our other external model parameters are midtropospheric values of vapor mixing ratio, CO_2 and radon, the properties of air entrained into the CBL, and the lapse rate above cloud base, which we need because we have not included a coupled cloud-layer model. We have considered two idealized ecosystems, forest (based on observations in Wisconsin) and grassland (using parameter

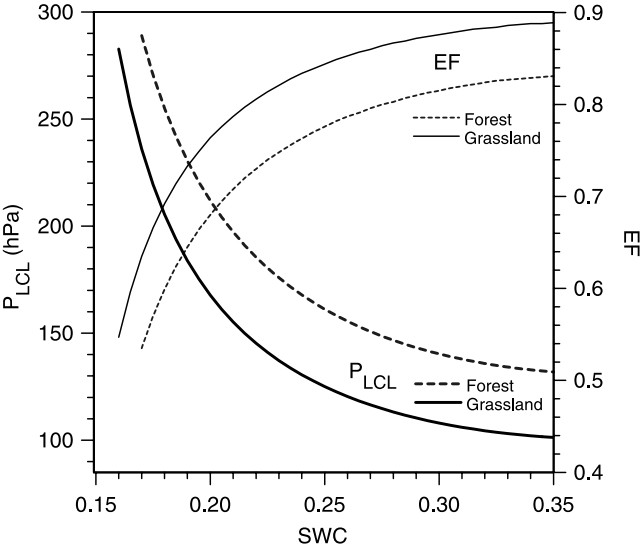

Figure 16. As in Figure 12 for forest and grassland. See color version of this figure in the HTML.

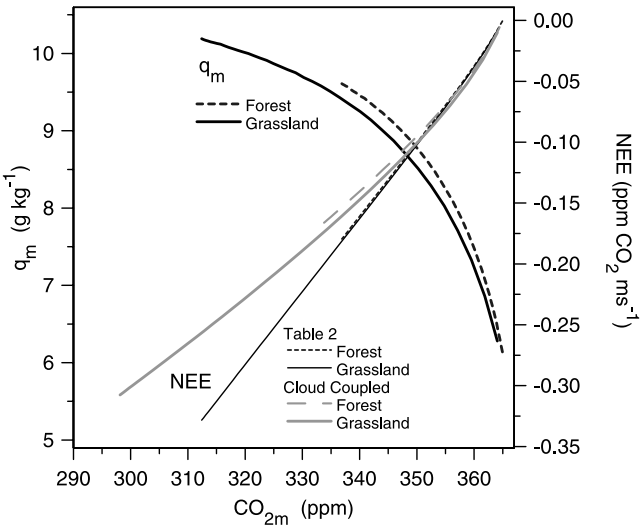

Figure 17. As in Figure 7b for forest and grassland. See color version of this figure in the HTML.

estimates from the literature) to show how the vegetation model affects the ML equilibrium.

[47] We vary external parameters in turn, keeping the others fixed with default values given in Table 2. A full range of SWC is always used, because this is a primary control on NEE in our simple vegetation model; on evaporation through stomatal resistance (R_{veg}), and hence on the surface energy balance. R_{veg} increases sharply, as SWC drops toward 0.137, the model "permanent wilting point," and the equilibrium depth of the ML increases sharply, as reduced evaporation leads to a warmer drier equilibrium. Increasing SW_{net} increases the depth of the ML, but has only a small impact on R_{veg} because of a cancellation of effects in the vegetation model for the Wisconsin forest system. We then showed the change of the surface energy fluxes and evaporative fraction with SW_{net}, both as a function of SWC and ML depth as a pressure thickness, P_{LCL}, as these representations present two quite different perspectives of the equilibrium of the fully coupled system. As a function of SWC, we see the impact of surface processes on evaporation (and NEE). However, the ML equilibrium is controlled more by the energy balance of the ML as a whole (not just the surface) and the coupling to the cloud layer and the entire CBL. Indeed we have formulated the ML upper boundary conditions for θ and q in terms of ML depth and the ML radiative cooling is a primary control on ML depth, and the surface sensible heat flux. Consequently the surface energy fluxes become linear as functions of P_{LCL} and the sensible heat flux varies little with SW_{net}. A similar simplification occurs for the ML θ_m, q_m and CO_{2m}. As a function of SWC, these ML values are nonlinear and show the warming and drying of the ML as SWC decreases and SW_{net} increases. However, ML θ_m, q_m have a nearly linear dependence on P_{LCL}, and a rather weak dependence on surface solar forcing. CO_{2m} has a nonlinear dependence on P_{LCL}, but this too depends only weakly on solar forcing, at least for the forest ecosystem parameters we have used. Only ML radon, for which we specified a constant surface flux, decreases strongly with increased solar forcing, since the mass exchange at the top of the ML increases with SW_{net}, reducing the gradient to the free troposphere. The model uses two mass exchanges: one at cloud base, determined by the equilibrium of the ML, and the condition that its top be at the LCL of air at the base of the ML; and a second, an entrainment at CBL top, necessary to give q equilibrium in the face of subsidence of dry air into the CBL. Both these mass fluxes and their difference, which can be considered an additional mass flux into clouds, increase with SW_{net}. As the ML deepens, it reaches a depth (around 280 hPa thickness) where this cloud mass flux disappears, and the model with the constraint that ML top also be cloud base becomes invalid. One general and important conclusion is that unless SWC becomes so low that the ML becomes very deep, the assumptions of the model can be satisfied, with cloud base at the top of the ML and a shallow cloud field above in balance with weak large-scale subsidence. *Betts* [2000] reached a similar conclusion from a simpler model. The cloud-coupled solutions, while more nonlinear, appear to be a useful generalization to show the qualitative impact of the cloud field on the ML equilibrium.

[48] We then considered the impact of changing q_t, the mixing ratio of air entering the CBL top. This has no impact on the thermodynamic structure and fluxes of the ML, but increasing q_t increases the derived mass exchange with the free troposphere, and therefore reduces the inferred cloud mass flux. Essentially the ML stays the same, a smaller cloud mass flux compensates for moister air entrained at CBL top, but the CBL will also tend to deepen faster, unless there is compensating subsidence. This has a large impact on the CO_{2m} and Rn_m, as these are passive tracers above the surface, and as the mass exchange with the free troposphere increases, they come closer to their values at CBL top. This changes the coupling between CO_{2m} and q_m, and between CO_{2m} and NEE, which is almost unaffected by the changes in CO_{2m}. This means, not surprisingly, that if we are to relate the moisture structure and fluxes to the CO_2 structure and NEE, we need to know both the mixing ratio and CO_2 content of air entrained into the CBL.

[49] We summarized the effect of varying stability above the ML, but we did not show figures, because the lack of a model for the cloud layer is a weakness of the model. Increasing stability has a direct effect on the thermodynamic equilibrium, and the ML gets warmer and moister; while the mass exchange at cloud base and with the free troposphere decrease, which leads to a higher ML radon. However, CO_{2m} changes relatively little, because NEE is also reduced as respiration increases with temperature, and this has a slightly larger impact than the reduction in vertical mixing. The coupling between CO_{2m} and q_m is greatly affected by increasing stability (because q_m increases), but the link between CO_{2m} and NEE is shifted only slightly. Our main conclusion is that a better thermodynamic model for the CBL is needed to give further insight into the links between temperature and humidity, radiation and stability. In an earlier paper over the tropical ocean, *Betts and Ridgway* [1989] used a mixing line parameterization to represent the shallow cloud field and a coupled radiation code to compute the cloud layer equilibrium. However, they simplified the problem, by using a moist adiabat to represent the vertical temperature structure of the deep tropics and constrained the energy balance within the tropics. Further developments of our model in this area are needed.

[50] In the absence of a coupled radiation code, we varied the radiative cooling of the ML, and also showed solutions where we coupled this radiative cooling to the net cloud mass flux. As a function of SWC, both EF and ML depth decrease as ML radiative cooling increases, and the mass exchanges at ML top and CBL top also decrease. As a function of ML depth, the ML equilibrium shifts to a slightly cooler drier state with higher CO_{2m}, while radon, as expected, increases as the vertical mass exchange decreases. The coupling between CO_{2m} and q_m is almost unaffected, while that between CO_{2m} and NEE changes because respiration decreases as the ML cools. In fact the response of the ML equilibrium to reduced radiative cooling of the ML is qualitatively similar to the response to increased surface radiative forcing.

[51] Our final sensitivity test shows the different equilibrium for two idealized ecosystems, forest and grassland. For our grassland, both photosynthesis and respiration are greater for the same SWC, SW_{net}, and surface temperature. As a function of SWC, EF increases for grassland and ML depth decreases, both a direct response to increased photosynthesis, and reduced R_{veg}, giving an ML that is cooler, moister, and has lower CO_{2m}. However, as a function of ML depth, the picture is much simpler. The ML θ_m, q_m, radon, all the mass fluxes, and energy fluxes are independent of ecosystem: the lower grassland R_{veg} gives a lower equilibrium depth, but the thermodynamic structure and fluxes depend only on this depth. The result is that, while the coupling between CO_2 and q_m depends on ecosystem, the coupling between CO_2 and NEE does not. This is clearly an important and useful result, because the ML integrates over the landscape, which will generally include multiple ecosystem types.

[52] Our equilibrium model is an oversimplification. The vegetation model is based on fitting data from a Wisconsin forest tower, and the characteristics of other ecosystems need to be explored in terms of our equilibrium model, as they may behave differently. At the surface we have represented photosynthesis and respiration and the surface energy fluxes (across the surface superadiabatic layer) in terms of 24-hour mean quantities. One obvious extension would be to average over day and night separately. We have done this, but the solutions are not qualitatively different, and the model is more complex, requiring additional assumptions for the nighttime BL and day-night storage of energy, so we do not present these solutions. The 24-hour mean model captures the essence of the long-term averaged ML state, and will, we believe, be useful in interpreting the slow evolution of the CBL over land on timescales longer than a day. Indeed, other work shows that the BL climate states over land and the coupling of processes at the surface in a fully time dependent model (the European Centre reanalysis) can be mapped with remarkable precision by the daily mean state and daily flux averages [*Betts*, 2004].

[53] ML variables are readily measurable, and are representative of large spatial scales, whereas the surface fluxes measured by eddy covariance techniques are representative of small spatial scales and especially difficult at night. Thus the ML variables may give estimates of the surface fluxes, averaged over large spatial scales, rather longer than the 24-hour mean advection distance (432 km at 5 ms^{-1}). At the same time they may give insight into optimum parameter sets for regional ecosystem models. The figures show that there is always a strong coupling between CO_{2m} and NEE, and between CO_{2m} and q_m, although there is dependence on the external boundary conditions of our model (some of which may also be measurable). In addition, ML radon is a sensitive measure of the mass exchange at cloud base. Consequently we think it likely that regional carbon budgets can be estimated or at least constrained using regional ML budgets, provided some upper air information of temperature, humidity, and CO_2 is available, and we are planning to do this in the future.

[54] This equilibrium model includes the impact of the LCL as a constraint on ML depth, and our cloud-coupled solutions have included in a simple form the radiative impact of clouds; since the coupling with the cloud field is a fundamental part of the ML equilibrium for water vapor, CO_2 and the radiation field. Certainly there are processes that our simple model neglects. The most important perhaps is precipitation from deep clouds, which evaporates and cools the ML, and plays a role in its long-term thermodynamic equilibrium [see *Betts*, 2000]; and at the surface precipitation evaporates from a wet canopy (which is uncoupled to photosynthesis and is not included in our transpiration model). During precipitation events the vertical mixing of the troposphere is typically extensive, and is not represented by our nonprecipitating CBL model. However, the periods of suppressed convection between rain episodes are temporally dominant, and it is during these periods that we expect our model to provide useful information. In a companion paper [*Helliker et al.*, 2004] we shall show that, during these episodes when subsidence dominates, the coupling between the moisture and CO_2 budgets is consistent with the model solutions in this paper and sufficient to provide a way of estimating NEE from evaporation, given the BL CO_2 and moisture structure. Furthermore, we extend this simple methodology by averaging through synoptic events to obtain estimates of NEE that agree with ground-based estimates over monthly timescales.

Appendix A: Relationship Between Relative Humidity (RH), Saturation Pressure, and Cloud Base

[55] RH has fundamental significance in the atmosphere, because of its tight relationship to saturation pressure, and hence to lifting condensation level (LCL) and cloud base (the critical level of the liquid phase transition, which affects radiative and microphysical processes). Because this link is generally not fully appreciated, often RH is often thought as being of lesser significance than the ''conserved'' mixing ratio. However, saturation pressure is conserved in dry and wet adiabatic processes [*Betts*, 1982], so that the saturation pressure of a ML is of fundamental importance. The equilibrium ML model shows the link between the availability of water for evaporation and equilibrium cloud base, which is just the saturation pressure or LCL of ML air. Figure A1 shows the relation between RH (as a decimal) and the height of the h_{LCL} (right-hand scale) as surface temperature varies, and (left-hand scale) the corresponding relationship with $P_{LCL}/p = (p - p^*)/p$, the pressure height to the saturation level, p^*, scaled by the pressure p. The dependence on temperature is weak. Formally, P_{LCL} is

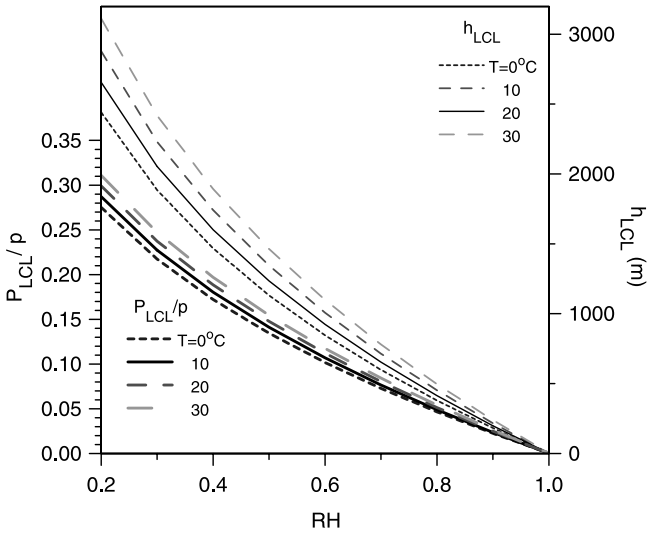

Figure A1. Relation between RH and the height of the lifting condensation level h_{LCL} (right-hand scale) as surface temperature varies, and the corresponding relationship with P_{LCL}/p (left-hand scale). See color version of this figure in the HTML.

directly related to (1 − RH) by the approximate linear formula [*Betts*, 1997]

$$P_{LCL}/p = (1 - RH)/\{A + (A - 1)RH\}, \qquad (A1)$$

where $A = (0.622\lambda/\{2C_p\ T\})$ decreases with increasing temperature from 2.83 at 0°C to 2.48 at 25°C; with λ the latent heat of vaporization and C_p the specific heat of air at constant pressure. Thus we may consider (1 − RH) as a measure of the vertical displacement of air from its saturation pressure, either before it has entered cloud in the ML, or higher in the troposphere where it has exited a cloud and sunk to buoyancy equilibrium. It is useful to keep in mind some characteristic values. Over the ocean, as is well known, typical cloud base height of 500 m or $P_{LCL} \approx$ 50 hPa, corresponds to RH ≈ 80%. Over Amazonia in the rainy season, afternoon cloud base may reach around 800 m, or $P_{LCL} \approx 80$ hPa with RH ≈ 70%. Over the boreal forest in spring, cloud base may reach around 2500 m, or $P_{LCL} \approx$ 200 hPa with RH ≈ 30%; while over a desert, where water is largely unavailable for evaporation, cloud base may be 3500 m, $P_{LCL} \approx 300$ hPa with RH ≈ 20% (or less). In our equilibrium model we see the range of solutions between $100 < P_{LCL} < 300$ hPa, as SWC varies. Equation (A1) can be inverted to give RH

$$RH = (1 - A\,P_{LCL}/p)/(1 + (A - 1)P_{LCL}/p). \qquad (A2)$$

In our model solution for the ML equilibrium, we shall use the slightly better quadratic empirical fit to find RH_m at the base of the ML

$$RH_m = 1 - (2A - 1.13)P_{LCL}/P_{sf} + A(A - 0.83)(P_{LCL}/P_{sf})^2, \qquad (A3)$$

where P_{sf} is the surface pressure. Then we can find ML mixing ratio (in g kg^{-1}) from RH_m, using

$$q_m = RH_m q_s(T_m)/\{1 + q_s(T_m)(1 - RH_m)/622\}. \qquad (A4)$$

This simplifies the solution of the coupled system. Similar relationships to (A3) and (A4) are used to link P_{LCLcld}, RH_{cld} and q_{cld} for air just above the ML.

[56] **Acknowledgments.** Alan Betts acknowledges support from NSF under grant ATM-9988618 and from NASA under grant NAS5-11578. J.B. and B.H. acknowledge support from NOAA grant GC00-280. This is CIW-DGE publication 44. We are grateful for discussions with Steve Wofsy and for suggestions from reviewers.

References

Bakwin, P. S., K. J. Davis, C. Yi, S. C. Wofsy, J. W. Munger, L. Haszpra, and Z. Barcza (2004), Regional carbon dioxide fluxes from mixing ratio data, *Tellus*, *Ser. B*, *56*, 301–311.

Ball, J. T. (1987), An analysis of stomatal conductance, 89 pp., Ph.D. thesis, Stanford Univ., Stanford, Calif.

Betts, A. K. (1973), Non-precipitating convection and its parameterization, *Q. J. R. Meteorol. Soc.*, *99*, 178–196.

Betts, A. K. (1975), Parametric interpretation of trade-wind cumulus budget studies, *J. Atmos. Sci.*, *32*, 1934–1945.

Betts, A. K. (1982), Saturation point analysis of moist convective overturning, *J. Atmos. Sci.*, *39*, 1484–1505.

Betts, A. K. (1997), The parameterization of deep convection, in *The Physics and Parameterization of Moist Atmospheric Convection*, *NATO ASI Ser. C*, vol. 505, edited by R. K. Smith, chap. 10, pp. 255–279, Kluwer Acad., Norwell, Mass.

Betts, A. K. (2000), Idealized model for equilibrium boundary layer over land, *J. Hydrometeorol.*, *1*, 507–523.

Betts, A. K. (2003), The diurnal cycle over land, in *Forests at the Land-Atmosphere Interface*, edited by M. Mencuccini et al., chap. 6, pp. 73–93, CABI, Wallingford, Oxon, UK.

Betts, A. K. (2004), Understanding hydrometeorology using global models, *Bull. Am. Meteorol. Soc.*, in press.

Betts, A. K., and W. Ridgway (1988), Coupling of the radiative, convective, and surface fluxes over the equatorial Pacific, *J. Atmos. Sci.*, *45*, 522–536.

Betts, A. K., and W. L. Ridgway (1989), Climatic equilibrium of the atmospheric convective boundary layer over a tropical ocean, *J. Atmos. Sci.*, *46*, 2621–2641.

Betts, A. K., M. L. Goulden, and S. C. Wofsy (1999), Controls on evaporation in a boreal spruce forest, *J. Clim.*, *12*, 1601–1618.

Betts, A. K., J. H. Ball, M. Bosilovich, P. Viterbo, Y.-C. Zhang, and W. B. Rossow (2003), Intercomparison of water and energy budgets for five Mississippi subbasins between ECMWF reanalysis (ERA-40) and NASA-DAO fvGCM for 1990–1999, *J. Geophys. Res.*, *108*(D16), 8618, doi:10.1029/2002JD003127.

Collatz, G. J., J. T. Ball, C. Grivet, and J. A. Berry (1991), Physiological and environmental regulation of stomatal conductance, photosynthesis, and transpiration: A model that includes a laminar boundary layer, *Agric. For. Meteorol.*, *54*, 107–136.

Cotton, W. R., G. D. Alexander, R. Hertenstein, R. L. Walko, R. L. McAnelly, and M. Nicholls (1995), Cloud venting—A review and some new global annual estimates, *Earth Sci. Rev.*, *39*, 169–206.

Davis, K. J., P. S. Bakwin, B. W. Berger, C. Yi, C. Zhao, R. M. Teclaw, and J. G. Isebrands (2003), The annual cycle of CO_2 and H_2O exchange over a northern mixed forest as observed from a very tall tower, *Global Change Biol.*, *9*, 1278–1293.

De Bruin, H. A. R. (1983), A model for the Priestley-Taylor parameter, α, *J. Clim. Appl. Meteorol.*, *22*, 572–578.

Denmead, O. T., M. R. Raupach, F. X. Dunin, H. A. Cleugh, and R. Leuning (1996), Boundary layer budgets for regional estimates of scalar fluxes, *Global Change Biol.*, *2*, 255–264.

Fitzjarrald, D. R. (2002), Boundary layer budgeting, in *Vegetation, Water, Humans and the Climate: A New Perspective on an Interactive System*, edited by P. Kabat et al., pp. 239–254, Springer-Verlag, New York.

Fitzjarrald, D. R., O. C. Acevedo, and K. E. Moore (2001), Climatic consequences of leaf presence in the eastern United States, *J. Clim.*, *14*, 598–614.

Helliker, B. R., J. A. Berry, P. S. Bakwin, A. K. Betts, K. J. Davis, A. S. Denning, J. R. Ehleringer, J. B. Miller, M. P. Butler, and D. M. Ricciuto (2004), Estimates of net CO_2 flux by application of equilibrium boundary layer concepts to CO_2 and water vapor measurements from a tall tower, *J. Geophys. Res.*, doi:10.1029/2004JD004532, in press.

Kim, J., and S. B. Verma (1990), Components of surface energy balance in a temperate grassland ecosystem, *Boundary Layer Meteorol.*, *51*, 401–417.

Kritz, M. A., S. W. Rosner, and D. Z. Stockwell (1998), Validation of an off-line three-dimensional chemical transport model using radon profiles: 1. Observations, *J. Geophys. Res.*, *103*, 8425–8432.

Kuck, L. R., et al. (2000), Measurements of landscape-scale fluxes of carbon dioxide in the Peruvian Amazon by vertical profiling through the atmospheric boundary layer, *J. Geophys. Res.*, *105*, 22,137–22,146.

Levy, P. E., A. Grelle, A. Lindroth, M. Molder, P. G. Jarvis, B. Kruijt, and J. B. Moncrieff (1999), Regional-scale CO_2 fluxes over central Sweden by a boundary layer budget method, *Agric. For. Meteorol.*, *99*, 169–180.

Lloyd, J., et al. (2001), Vertical profiles, boundary layer budgets, and regional flux estimates for CO_2 and its $^{13}C/^{12}C$ ratio and for water vapor above a forest/bog mosaic in central Siberia, *Global Biogeochem. Cycles*, *15*, 267–284.

McNaughton, K. G., and T. W. Spriggs (1986), A mixed-layer model for regional evaporation, *Boundary Layer Meteorol.*, *34*, 243–262.

Monteith, J. L. (1977), Climate and the efficiency of crop production in Britain, *Philos. Trans. R. Soc. London, Ser. B*, *281*, 277–294.

Monteith, J. L. (1981), Evaporation and surface temperature, *Q. J. R. Meteorol. Soc.*, *107*, 1–27.

Raupach, M. R. (1995), Vegetation-atmosphere interaction and surface conductance at leaf, canopy, and regional scales, *Agric. For. Meteorol.*, *73*, 151–170.

Raupach, M. R. (2000), Equilibrium evaporation and the convective boundary layer, *Boundary Layer Meteorol.*, *96*, 107–141.

Raupach, M. R. (2001), Combination theory and equilibrium evaporation, *Q. J. R. Meteorol. Soc.*, *127*, 1149–1181.

Raupach, M. R., O. T. Denmead, and F. X. Dunin (1992), Challenges in linking atmospheric CO_2 concentrations to fluxes at local and regional scales, *Aust. J. Bot.*, *40*, 697–716.

Salisbury, F. B., and C. W. Ross (1992), *Plant Physiology*, Wadsworth, Belmont, Calif.

Tennekes, H. A. (1973), Model for the dynamics of the inversion above a convective boundary layer, *J. Atmos. Sci.*, *30*, 558–567.

J. Berry and B. Helliker, Department of Global Ecology, Carnegie Institution of Washington, Stanford, CA 94305, USA.

A. K. Betts, Atmospheric Research, 58 Hendee Lane, Pittsford, VT 05763, USA. (akbetts@aol.com)